NMR Relaxation Studies of Fluorinated Drugs

Aditya Jhajharia

A dissertation submitted for the partial fulfilment of
BS-MS dual degree in Science

Indian Institute of Science Education and Research Mohali
April 2014

Certificate of Examination

This is to certify that the dissertation titled **"NMR Relaxation Studies of Fluorinated Drugs"** submitted by **Mr. Aditya Jhajharia** (Reg. No. MS09008) for the partial fulfilment of BS-MS dual degree programme of the Institute, has been examined by the thesis committee duly appointed by the Institute. The committee finds the work done by the candidate satisfactory and recommends that the report be accepted.

Prof. Arvind | Prof. K. S. Viswanathan | Dr. Kavita Dorai (Thesis supervisor)

Dated: April 25^{th}, 2014

Declaration

The work presented in this dissertation has been carried out by me under the guidance of Dr. Kavita Dorai at the Indian Institute of Science Education and Research Mohali.

This work has not been submitted in part or in full for a degree, a diploma, or a fellowship to any other university or Institute. Whenever contributions of others are involved, every effort is made to indicate this clearly, with due acknowledgement of collaborative research and discussions. This thesis is a bonafide record of original work done by me and all sources listed within have been detailed in the bibliography.

Aditya Jhajharia

Dated : April 25^{th}, 2014

In my capacity as the supervisor of the candidate's project work, I certify that the above statements by the candidate are true to the best of my knowledge.

Dr. Kavita Dorai
(Thesis supervisor)

Acknowledgment

At the first place, I would like to express my deep gratitude and thanks to Dr. Kavita Dorai for her guidance and encouragement. I would also like to thank IISER Mohali for providing me with the infrastructure and facilities during the tenure of my project.

I am much thankful to my thesis committee members Prof. Arvind and Prof. K. S. Viswanathan for their valuable inputs and support.

I am thankful to Prof. N. Sathyamurthy, Director IISER Mohali for his kind support and encouragement. I am grateful to Prof. Arvind for his motivation and inspiration. He has been of immense help throughout my stay at IISER Mohali.

My sincere thanks to Shruti Dogra and Navdeep Gogna for their help in teaching me various things about NMR and for their helpful discussions. I must mention my dear friend, Abhishek Mishra who has been the go-to guy throughout my stay. I would like to thank my lab members Harpreet, Debmalaya, Amandeep, Satnam for maintaining a friendly environment.

I am indebted to Prof. R. V. Hosur, TIFR Mumbai and Prof. K. V. Ramanathan, IISc Bangalore for their guidance, support and for motivating me to work in the field of NMR Spectroscopy.

My special thanks to Adhikar, Aditya, Anuj, Shiv Charan, Akash, Karishma and other friends for their help and cheerful moments during my stay in the campus.

Though impossible to express in words, I owe my deepest gratitude and thankfulness to my parents and my sister for being the best, most supportive, encouraging, patient and loving teachers and guides throughout my whole life. Without them, my current life would not be this wonderful and adventurous experience.

And finally i want to thank God for giving me a definite goal in my life.

List of Figures

List of Tables

Abbreviations

NMR	**N**uclear **M**agnetic **R**esonance
^{1}**H**	**1 H**ydrogen
^{13}**C**	**13 C**arbon
^{19}**F**	**19 F**luorine
^{31}P	**31 P**hosphorous
M	**M**agnetization
N	**N**umber of spins
1D	**1 D**imensional
2D	**2 D**imensional
COSY	**CO**rrelations **S**pectroscop**Y**
HSQC	**H**eteronuclear **S**ingle **Q**uantum **C**oherence
HMBC	**H**eteronuclear **M**ultiple **B**ond **C**orrelation
HMQC	**H**eteronuclear **M**ultiple **Q**uantum **C**orrelation
NOE	**N**uclear **O**verhauser **E**ffect
NOESY	**N**uclear **O**verhauser **E**ffect **S**pectroscop**Y**
DOSY	**D**iffusion **O**rdered **S**pectroscop**Y**
PFGSE	**P**ulsed **F**ield **G**radient **S**pin **E**cho
DPPC	**D**i **P**almitoyl **P**hosphatidyl **C**holine
FID	**F**ree **I**nduction **D**ecay
CSA	**C**hemical **S**hift **A**nisotropy

Contents

Abstract

Fluorine plays an important role in estimating the binding affinity and potency of drugs. This thesis work focuses on the study of fluoroquinolones which are used to treat bacterial infections such as respiratory and urinary tract infections. DNA gyrase is the target site for the quinolones. These fluoroquinolones bind to these enzymes and inhibit their activity. In this work, relaxation and diffusion studies were done for these drugs and similar molecular mass compounds could be differentiated using diffusion study. Here, diffusion study of Pazufloxacin and Prulifloxacin were done inside DPPC lipid bilayer.Their diffusion studies tells us about their interaction with the DPPC lipid bilayer and their motion in the solution.

^{19}F chemical shift anisotropy (CSA) tensor is a useful tool in NMR to characterize biomolecules. This work focuses on the characterization of CSA tensor of fluorine in fluoroquinolones using liquid state NMR cross-correlated relaxation experiments and quantum computational methods. The experiments are used to characterize the CSA tensor magnitude and its orientation, through measurement of cross-correlated spin relaxation rates between several different relaxation pathways in these molecules.

Chapter 1 deals with a short introduction to NMR, its relaxation phenomenon and basics of computational chemistry. Chapter 2 focusses on relaxation and diffusion studies of drugs Pazufloxacin and Prulifloxacin. It involves experimentally calculated relaxation times and diffusion coefficients for these drugs using DPPC. Chapter 3 involves experimental analysis of Fluoroquinolones using 1-D and 2-D based experiments. Lastly, Chapter-4 includes introduction to CSA tensor and use of quantum chemistry calculations to characterise these CSA tensors. Cross correlated spin relaxation liquid-state NMR experiments were performed to calculate fluorine CSA tensor.

Chapter 1

Basics of Nuclear Magnetic Resonance

1.1 Nuclear Magnetism

Nuclear magnetism is a vector quantity, firstly observed in the electron. It is a phenomenon of the existence of a nuclear spin angular momentum I.[3] and angular momentum is defined as a quantity possessed by a rotating object. Spin is a fundamental property of all subatomic particles, including the proton or the neutron, as well as objects built from them. The magnitude of I is given by the expression.[4]

$$|I| = \sqrt{I(I+1)\hbar} \tag{1.1}$$

where $\hbar = h/2\pi$ is reduced Planck constant.[5] Spin angular momentum is characterized by the nuclear spin quantum number. A nuclear spin quantum number I can be either integer or half-integer. Nuclei with odd or even atomic number and odd mass number have half integer or integer spin quantum number. In NMR spectroscopy, the most important nuclei are those with $I = 1/2$ (spin-1/2 nuclei), such as some stable isotopes ^{1}H, ^{13}C or ^{19}F or ^{15}N. Nuclei with even atomic number and even mass number have zero spin quantum number and spin zero nuclei can not be detected by using NMR. Nuclei with spin $I > 1/2$ are called quadrupolar nuclei. They have nonspherical distribution of electric charge, which gives them electric quadrupole moment. Quadrupolar nuclei have broad lines, which causes rapid relaxation and thus its observation is difficult to study.[6]

In the presence of arbitrary direction, I is quantized. It can be understood by taking

an example of a diatomic molecule:

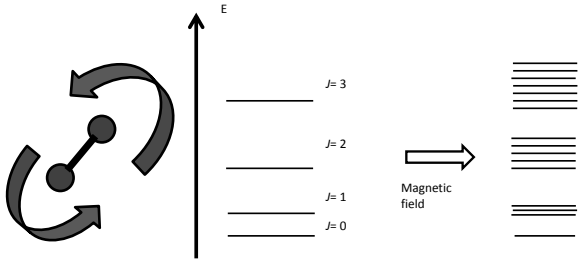

Figure 1.1: A rotating diatomic molecule and its energy levels

In NMR, this direction is determined by the strong static magnetic field B_0 which is along z-direction. Due to quantized spin angular momentum vector, z-component has discrete possible values. The z-component of I is given by[4]

$$I_z = m\hbar \tag{1.2}$$

where m is the magnetic quantum number m= (-I, -I+1, ..., I-1, I) with 2I+1 discrete possible values.

Nuclei with non-zero spin angular momentum produce nuclear magnetic moments. Spin angular momentum and the magnetic moment are proportional to each other. Thus, it is given by the relation[4]

$$\mu = \gamma I \tag{1.3}$$

where γ is gyromagnetic ratio.[7] It is a constant quantity for each nucleus and it be positive or negative. So, μ and I are parallel or antiparallel to each other.

Nuclei with non-zero spin are detected by NMR. When an ensemble of nuclei interacts with an external magnetic field, the nuclear spins distribute themselves into non-degenerate discrete energy levels in accordance with the Boltzmann law of population distribution. For example: Nuclei with spin half when placed in a magnetic field B_0 interact with the magnetic field and arrange themselves into α and β energy levels, populating these two energy levels according to the Boltzmann law of popula-

tion distribution which is given by:

$$\frac{N_\beta}{N_\alpha} = \exp(-\frac{(E_\beta - E_\alpha)}{k_B T}) \tag{1.4}$$

where N_β and N_α are the number of spins in the α and β energy levels respectively, k_B is the Boltzmann constant and T is the thermodynamic temperature of the spin system.

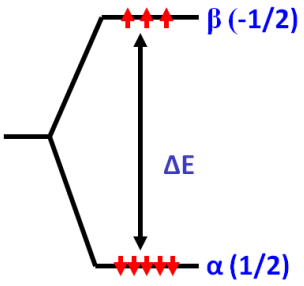

Figure 1.2: Energy distribution of spin 1/2 in the presence of external magnetic field

The Figure 1.2 shows the energy distribution of spins for a system with spin half nuclei in the presence of external magnetic field. Magnified impact of redistribution of spins in α and β spins on application of magnetic field has been shown. The frequency corresponding to the difference between two α and β energy levels is the product of the gyromagnetic ratio of the observed nuclei and the strength of applied magnetic field and is called the Larmor precession frequency of the nuclei. This is given by:

$$\omega = -\gamma B_0 \tag{1.5}$$

Magnetic substances do interact with the magnetic fields. Interaction is given in terms of magnetic moment μ. In the presence of the external magnetic field, energy of spin states depends on the interaction between its magnetic moment and B_0 and is given by:

$$E = -\mu \cdot B = -\gamma I \cdot B \tag{1.6}$$

Energy expression depends on the relative direction of the B and μ. When magnetic moment μ is parallel to the field B, energy will be lowest. In NMR, field B is equal to the applied external magnetic field B_0 in the z-direction. Energy can be written

by using Eq.1.2

$$E_m = -\gamma I_z B_0 = -\gamma m \hbar B_0 \tag{1.7}$$

There are $2I+1$ equally spaced energy levels possible, which are called Zeeman energy levels and the difference in energy between the α and β states (spin 1/2 nuclei) is given by

$$\Delta E = \gamma \hbar B_0 \tag{1.8}$$

It is the difference in the population of the nuclear spins in any two adjacent energy states which gives rise to the net magnetization of the sample. The redistribution of the net magnetization can be done by applying a radio frequency pulse whose frequency matches with the Larmor precession frequency of the nuclei.

At equilibrium, population of spin energy states are unequal and lower energy states are highly populated than higher energy states. The relative populations of the energy states are given by the Boltzmann distribution[4] :

$$\frac{N_m}{N} = \frac{\exp(-E_m/k_B T)}{\sum_{m=-I}^{I} \exp(-E_m/k_B T)} = \frac{\exp(-\gamma m \hbar B_0/k_B T)}{\sum_{m=-I}^{I} \exp(-\gamma m \hbar B_0/k_B T)} \approx \frac{1}{2I+1}(1+\frac{m\hbar\gamma B_0}{k_B T}) \tag{1.9}$$

where N_m is the number of nuclei in the m^{th} state, N is total number of spins, T is absolute temperature. The final expression of the equation is obtained by applying Taylor series expansion. The populations of the states depend on the applied magnetic field strength. As field strength increases, population difference between the states also increase because of larger energy levels. NMR spectroscopy is based on ensemble of nuclear spins and the bulk nuclear magnetic moment $\vec{M}$ is given by the vector sum of μ_i of the individual nuclei:

$$M = \sum_{i=1}^{N} \mu_i \tag{1.10}$$

Using Eqs. (1.2),(1.3), (1.9), the equilibrium value M_0 of the z-component of M (bulk z-magnetization) in the field of B_0 is given by:

$$M_0 = \gamma \hbar \sum_{m=-I}^{I} m N_m \approx N \gamma^2 \hbar^2 B_0 I(I+1)/3k_B T \tag{1.11}$$

The selection rule for magnetic dipole transitions is $m = \pm 1$. The sensitivity of NMR spectroscopy depends upon the population differences and strong magnetic field required to obtain higher sensitivity.

1.2 Relaxation Phenomenon

Relaxation of a perturbed spin system at thermal equilibrium is well known in all spectroscopy. Relaxation in NMR is unusually slower than other spectroscopy or other molecular energy levels. For example, an excited electronic energy states have lifetime of few microseconds, vibrational and rotational energy levels have lifetime of few nanoseconds but in NMR, to return to the equilibrium magnetization the time can be between milliseconds and seconds.[1]

A pulse can be understood as simply turning on Radio frequency (RF) radiation of defined amplitude for a time period and then switching it off. Completely defined by phase, amplitude, duration and the central frequency where it is applied, the RF pulse imposes a torque on the net magnetization vector in a direction perpendicular to the direction of B_1 field that rotates the bulk magnetization vector from the z-axis to the xy plane.

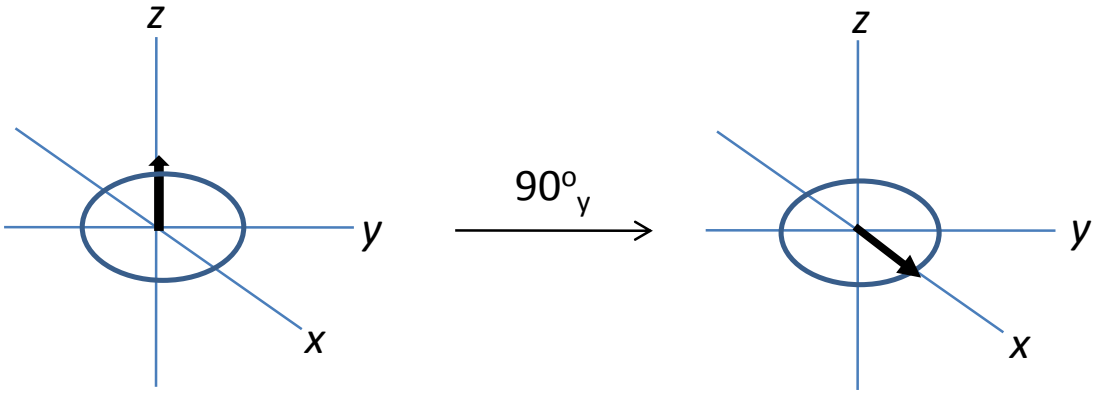

Figure 1.3: 90^0_y pulse is applied to the z-magnetization which convert the magnetization in the x-axis.

As it can be seen from the illustration, a 90^0 pulse brings the bulk magnetization vector to x axis, creating transverse magnetization in which the phases of the individual spin precession frequencies are correlated. The system is in a non-equilibrium

state and needs to relax back into the equilibrium state. This is achieved by two relaxation processes, longitudinal and transverse relaxation. Relaxation is the process by which the magnetization returns to its equilibrium position. At equilibrium there is no transverse magnetization and so only the z-magnetization exist. In this process z-magnetization returns to its equilibrium value and transverse magnetization decays from equilibrium value to zero.

When the bulk magnetization is rotated away from z-axis, the energy of the spin is increased because low energy arrangement of the spins are along Z-axis and spins need to loss their energy to come back to equilibrium. The process by which z-magnetization returns to its equilibrium value is called longitudinal relaxation or spin-lattice relaxation. It is also called spin-lattice relaxation because it occurs due to the interaction of spins with their environment. The longitudinal relaxation time constant T_1 is determined by the inversion recovery experiment. The process by which transverse component of magnetization vector M_{xy} exponentially decays towards its equilibrium value of zero is called spin-spin relaxation. It is caused by spins when they interact with themselves.[1,6] The transverse relaxation time constant T_2 is determined by the spin echo experiment. Experimental details of T_1 and T_2 are discussed in the next chapter.

The equilibrium magnetization depends on the number of spins, their gyromagnetic ratio and the magnitude of the applied field. Each spin has a magnetic moment and the magnetic moments of the individual spins determine the bulk magnetization of the sample which is a vector quantity having magnitude (determined by gyromagnetic ratio) and direction. Magnetic moment of each spin generates it own magnetic field. Therefore spins experience both applied magnetic field and field due to nearby spins. The field generated by the nearby spin is called *local field*. This *local field* is depends on the orientation of the spins. Local field affects the magnitude and orientation of the bulk magnetization.

Individual magnetic moments change orientation by interacting with an oscillating transverse magnetic field and all components (x,y,z) of the magnetic moments can be changed. Therefore local fields drive both transverse and z-magnetization to its equilibrium value and this is called the non-secular contribution to transverse relaxation. There is also an other way in which transverse magnetization driven to its equilib-

rium. Each spin experiences some different local field and so each spin is precesses at a slightly different frequency. Therefore spins go out of phase with one another and the transverse magnetization shrinks. This is called secular contribution to transverse relaxation. It is effected by the rate of the molecular motion. If the molecular motion is fast, spins very often experience changing local field and the spin precession frequency is determined by the time average of this local field. At fast molecular motion the time average of the local field is approximately same for all spins. Hence there will be small spreading of precession frequencies which results in less dephasing and slower transverse relaxation. If the molecular motion is slow, local field experienced by a particular spin also changes slowly and the time average of the spin precession frequencies is different for each spin. Results more spreading in local fields and it causes fast relaxation.[1]

1.3 Relaxation mechanism

Local field can change magnitude and orientation of the bulk magnetization, so it affects the relaxation. A source of local magnetic field is called a relaxation mechanism.[1] For spin-half nuclei, dipolar and chemical shift anisotropy mechanisms are dominant.

1.3.1 Dipolar Coupling

In an ensemble of spins every nucleus possesses a magnetic moment, these magnetic moments interact with each other through space, this interaction is known as dipolar coupling. So dipolar coupling arises due to the direct interaction between two particles with non-zero spin. In solution, the dipole-dipole interaction is averaged to its isotropic value by molecular tumbling but in solid state these interactions are not averaged. Due to this solid state NMR shows line broadening. The local field due to neighbouring spin depends on the distance r between the two spin, inversely proportional to r^3 and on molecular orientation of two spins relative to the applied magnetic field. It depends on gyromagnetic ratio of the spin,it is seen that larger the gyromagnetic ratio, larger is the magnetic moment and hence larger the local field. Dipolar coupling interaction can be between two same spins or different spins.
Dipolar coupling Hamiltonian interaction is given by-

$$H_{IS} = -d(3/cos^2\theta - 1)I_z S_z \tag{1.12}$$

parameter d is diploar coupling constant is given by

$$d = (\mu_0/4\pi)\hbar\gamma_I\gamma_S/r_{IS}^3$$

, where γ_I and γ_S are gyromagnetic ratio of spin I and spin S.

1.3.2 Chemical shift anisotropy

In presence of a strong applied magnetic field, electrons in the molecule give rise to a small induced field at the nucleus. This field is opposite to the applied field. So nucleus experiences some different magnetic field from a given magnetic field depending on their environment. This shifting in the larmor frequency depends on the size of the induced field. This shifting in the resonance frequencies are called chemical shifts.

$$B_j^{loc} = B_0 + B_j^{induced} \tag{1.13}$$

where B_j^{loc} is the magnetic field experienced by nuclei, B_0 is the static magnetic field and $B_j^{induced}$ is the magnetic field produced by electron clouds, j denotes the nuclei at site j. Field $B_j^{induced}$ is 10^{-4} times less than the static magnetic field. Local field varies as the molecule tumbles depends on the anisotropy of the chemical shift. Local field can be in any direction so this local field is a relaxation mechanism. The local field due to chemical shift is proportional to applied magnetic field. The magnitude of the induced field $B_j^{induced}$ is directly proportional to the applied magnetic field B_0 and is given by:-

$$B_j^{induced} = \delta^j \cdot B_0 \tag{1.14}$$

δ^j is called the chemical shift tensor of I_j and it is represented by a 3×3 matrix.

Chemical shift depends on the orientation of the molecule with respect to applied magnetic field, this is called chemical shift anisotropy. In liquid samples the molecules are tumbling so rapidly that the nuclei can see an average local field, hence have an average chemical shift, this is called isotropic chemical shift. It is given by:-

$$\delta_j^{iso} = \frac{1}{3}(\delta_{xx}^j + \delta_{yy}^j + \delta_{zz}^j) \tag{1.15}$$

where x, y, z is represented by principal axis system (PAS) and δ_{xx}^j, δ_{yy}^j, δ_{zz}^j are the principal component of the chemical shift anisotropy tensor at site j.

The chemical shift anisotropy (CSA) is given by:-

$$\delta_j^{aniso} = \delta_j^{zz} - \delta_j^{iso} \tag{1.16}$$

where δ_{xx}^j, δ_{yy}^j, δ_{zz}^j follow Herzfeld Berger convention for the magnitude, which is following

$$\delta_{zz}^j \geq \delta_{yy}^j \geq \delta_{xx}^j \tag{1.17}$$

The difference between other principal values is quantified by asymmetry η_j, which is defined by

$$\eta_j = \frac{\delta_{yy}^j - \delta_{xx}^j}{\delta_j^{aniso}} \tag{1.18}$$

where η_j is a dimensionless quantity between 0 to 1. Chemical shift tensor δ can be defined as sum of isotropic, antisymmetric, symmetric tensor which are tensor of rank 0,1,2 respectively.

$$\delta = \delta^{iso} + \delta^{sym} + \delta^{anti} \tag{1.19}$$

where

$$\delta^{iso} = \begin{bmatrix} (\delta_{xx} + \delta_{yy} + \delta_{zz})/3 & 0 & 0 \\ 0 & (\delta_{xx} + \delta_{yy} + \delta_{zz})/3 & 0 \\ 0 & 0 & (\delta_{xx} + \delta_{yy} + \delta_{zz})/3 \end{bmatrix}$$

$$\delta^{anti} = \begin{bmatrix} 0 & (\delta_{xy} - \delta_{yx})/2 & (\delta_{xz} - \delta_{zx})/2 \\ -(\delta_{xy} - \delta_{yx})/2 & 0 & (\delta_{yz} - \delta_{zy})/2 \\ -(\delta_{xz} - \delta_{zx})/2 & -(\delta_{yz} - \delta_{zy})/2 & 0 \end{bmatrix}$$

$$\delta^{sym} = \begin{bmatrix} \delta xx - (\delta_{xx} + \delta_{yy} + \delta_{zz})/3 & (\delta_{xy} + \delta_{yx})/2 & (\delta_{xz} + \delta_{zx})/2 \\ (\delta_{xy} + \delta_{yx})/2 & \delta yy - (\delta_{xx} + \delta_{yy} + \delta_{zz})3 & (\delta_{yz} + \delta_{zy})/2 \\ (\delta_{xz} + \delta_{zx})/2 & (\delta_{yz} + \delta_{zy})/2 & \delta zz - (\delta_{xx} + \delta_{yy} + \delta_{zz})3 \end{bmatrix}$$

where δ^{iso} does not change by rotation of the molecule, δ^{anti} causes spin relaxation and δ^{sym} after diagonalisation gives the principal axes δ_{xx}, δ_{yy}, δ_{zz}. In liquids, the rotational diffusion leads to the averaging of the the various parts of the CSA tensor(symmetric as well as asymmetric)and so because of this only δ_{iso} is observable in the resultant NMR spectra.Diagonal elements are not present in the asymmetric part of the CSA tensor and so we only get the perpendicular part of the static magnetic field.So the tilting produced in the local field is very little.This titling bring about a

second order effect in the resonance frequency whose value is quite small to be measured.

There are various NMR techniques through which we can calculate the CSA tensor.[8] In the most used method[9] , we take a single crystal and then we observe the resonance frequencies of the various sites in that crystal as functions of the orientation of the crystal with respect to the static magnetic field.The trajectories of the resonance frequencies leads to the principal values and principal axes of the CSA tensor. Better results can be obtained by using this technique but it is a fairly time taking process and requires single crystals. In an another approach, in the molecular frame, the principal direction of a CSA tensor can be calculated using the power spectra that is sensitive to the relative orientations of the CSA tensor of the nearby molecules.[10,11,12] The last few years has advanced the study of *ab initio* calculations of CSA tensors and many new methods involving density functional theories has contributed largely in the process.[13,14]

Chemical shift Hamiltonian can be written as-

$$H_{CS} = \gamma B_0 I_z[\delta_{iso} + 1/2\delta_{CSA}(3cos^2\theta - 1)] \tag{1.20}$$

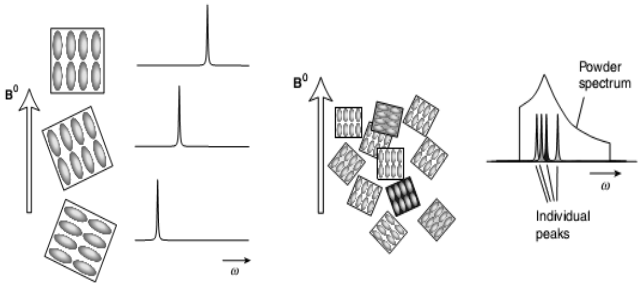

The illustration shows that due to change in orientation, larmor frequency changes and due to this in solid state peak will broad. In a rapidly tumbling molecule all possible orientations of the ellipsoid are sampled causing the orientation-dependent term to average to zero and leaving only the isotropic component of the chemical shift $\delta_{iso}\gamma B_0 I_z$, which is observed in liquid-state NMR spectra.

1.3.3 Relaxation by paramagnetic species

In the dipolar mechanism the source of the local field is the magnetic moments of other nuclear spins in the sample. Local magnetic field can be generated by unpaired electrons also. So unpaired electrons are also a source of a relaxation. The magnetic moment of the electron is very much greater than the proton, so the local field generated by an electron is much greater. Therefore, unpaired electrons are also a significant source of relaxation.

1.4 Describing random motion

Random thermal motion provides important time dependence to the local fields. A molecule can be distinct in two kind of motion: vibration and rotation. The rotation of the molecule will affect both diploar interaction and CSA, therefore these type of motion can be a source of relaxation. These motion are described by correlation functions.

1.4.1 Correlation function

The correlation function characterizes the time dependence of the random motion in sample. This function tells about the motion present at the Larmor frequency. Suppose a particular spin i experiences a local field $B_{loc,i}(t)$ which depends on time, so that at a time τ later the local field is $B_{loc,i}(t+\tau)$. The correlation function G(t, τ) is defined by as the average over the sample of the product $B_{loc}(t)B_{loc}(t+\tau)$:

$$\begin{aligned} G(t,\tau) &= \frac{1}{N}[B_{loc,1}(t)B_{loc,1}(t+\tau) + B_{loc,2}(t)B_{loc,2}(t+\tau) + ...] \\ &= \frac{1}{N}\sum_{i=1}^{N} B_{loc,i}(t)B_{loc,i}(t+\tau) \\ &= \overline{B_{loc}(t)B_{loc}(t+\tau)} \end{aligned} \tag{1.21}$$

The correlation function varies with τ and it starts at a maximum at $\tau = 0$ and goes to zero with higher value. So G(0) is given by -

$$\begin{aligned} G(0) &= \overline{B_{loc}(t)B_{loc}(t)} \\ &= \overline{B_{loc}^2} \end{aligned} \tag{1.22}$$

The exact form the correlation function depends on the interaction between the molecules and solvent. The correlation function is given with an exponential whose decay rate is set by τ:

$$G(\tau) = \overline{B_{loc}^2} \exp(-|\tau|/\tau_c)$$

Smaller the time correlation time faster G(τ) decays. This function is depends on the module of the time τ and exponential part of the correlation function is independent of the source of local fields which determines magnitude of G(τ).[1]

1.4.2 Spectral Density

As already discussed, molecular motion changes from time to time and resulting local field depends on the time. This molecular motion can be determined by a correlation function. The correlation function is a function of time, if we do Fourier transform , we obtain a function of frequency and the spectrum will tell intensity which is there at each frequency or motion present at the required frequency. The Fourier transform of the correlation function is called the *spectral density* and from this, amount of motion can be found at larmor frequency. So amount of motion at larmor frequency is found evaluating $J(\omega)$ at $\omega = \omega_0$.
Fourier transform of the exponential correlation function is:

$$\overline{B_{loc}^2} \exp(-|\tau|/\tau_c) \rightarrow \overline{B_{loc}^2} \frac{2\tau}{1+\omega^2\tau^2}$$

so

$$J(\omega) = \overline{B_{loc}^2} \frac{2\tau}{1+\omega^2\tau^2} \tag{1.23}$$

The spectral density at Larmor frequency as a function of the correlation time $J(\omega_0)$ and it will determine the rate of longitudinal relaxation. $J(\omega_0)$ will be maximum when $\omega_0\tau_c = 1$ and rate of the longitudinal relaxation will be maximum at $\tau_c = 1/\omega_0$.

1.5 Longitudinal relaxation of isolated spins

Magnetic moment of a single-half spins can point in any direction. Energy of these spins depends on angle between the magnetic moment and the applied field. When magnetic field is applied spin half will split into two energy levels as α and β. α and β are low and high energy levels and population will distribute into these two levels according to Boltzmann law of distribution. Population associated with α and

β levels are n_α and n_β.

Rate of transition from α to β is proportional to the population of α state, n_α:

$$\text{rate from } \alpha \text{ to } \beta = W_{\alpha\to\beta} n_\alpha$$

where $W_{\alpha\to\beta}$ is rate constant. Similarly,

$$\text{rate of transition from } \beta \text{ to } \alpha = W_{\beta\to\alpha} n_\beta$$

Transition from α to β decrease the population of α state and transition from β to α state increase the population of α state. Total rate of change of the population of the α state is:

$$\frac{dn_\alpha}{dt} = +W_{\beta\to\alpha} n_\beta - W_{\alpha\to\beta} n_\alpha \tag{1.24}$$

Similarly we can write, total rate change of the population of the β state:

$$\frac{dn_\beta}{dt} = +W_{\alpha\to\beta} n_\alpha - W_{\beta\to\alpha} n_\beta \tag{1.25}$$

At equilibrium, population will be constant so rate of change will be zero. Applying these condition on Eq.1.24 and 1.25

$$0 = +W_{\beta\to\alpha} n_\beta^0 - W_{\alpha\to\beta} n_\alpha^0, \qquad 0 = +W_{\alpha\to\beta} n_\alpha^0 - W_{\beta\to\alpha} n_\beta^0$$

by this equation

$$\frac{n_\alpha^0}{n_\beta^0} = \frac{W_{\beta\to\alpha}}{W_{\alpha\to\beta}} \tag{1.26}$$

At equilibrium rate of change of forward and rate of change of backward direction is same $W_{\beta\to\alpha} = W_{\alpha\to\beta}$ so it gives $n_\alpha^0 = n_\beta^0$. Population at equilibrium will be same for both levels.

We need to rewrite the equation for rate change

$$\textit{rate of change of } n_\alpha = W_{\alpha\beta}(n_\beta - n_\beta^0) - W_{\alpha\beta}(n_\alpha - n_\alpha^0) \tag{1.27}$$

$$\textit{rate of change of } n_\beta = -W_{\alpha\beta}(n_\beta - n_\beta^0) + W_{\alpha\beta}(n_\alpha - n_\alpha^0) \tag{1.28}$$

$n_\alpha - n_\alpha^0$ and $n_\beta - n_\beta^0$ are the deviation of population from equilibrium. If $n_\alpha = n_\alpha^0$, $n_\beta = n_\beta^0$ then rate of change of both n_α and n_β will be zero.

Z-magnetization is given by difference between population of α and β energy state so rate of change of z-magnetization is given by:

rate of change of M_z= rate of change of n_α - rate of change of n_β

$$\begin{aligned} \textit{Rate of change of } M_z \quad &= 2W_{\alpha\beta}(n_\beta - n_\beta^0) - 2W_{\alpha\beta}(n_\alpha - n_\alpha^0) \\ &= -2W_{\alpha\beta}[(n_\alpha - n_\beta) - (n_\alpha^0 - n_\beta^0)] \\ &= -2W_{\alpha\beta}(M_z - M_z^0) \end{aligned} \tag{1.29}$$

So rate of change of z-magnetization is given by:

$$\frac{dM_z(t)}{dt} = -R_z[M_z(t) - M_z^0] \tag{1.30}$$

where R_z is rate constant for longitudinal relaxation is equal to $2W_{\alpha\beta}$. Rate constant is also defined as $R_z = \dfrac{1}{T_1}$ and this time constant is called T_1 relaxation.

After integration and taking exponential of this equation, we get

$$M_z(t) = [M_z(0) - M_z^0]\exp(-R_z t) + M_z^0 \tag{1.31}$$

Inversion-recovery experiment is used for rate constant of longitudinal relaxation,. Pulse sequence of this experiment is first 180^0 pulse and after variable τ delay 90^0 pulse is applied. First 180^0 pulse invert the z-magnetization to -z direction, so that $M_z(0)$= -M_z^0 and the magnetization is allowed to relax for a delay time τ. Using Eq.2.2 z-magnetization at time τ is given by:

$$\begin{aligned} M_z(\tau) = \quad & -2M_z^0\exp(-R_z\tau) + M_z^0 \\ = \quad & M_z^0[1 - 2\exp(-R_z\tau)] \end{aligned} \tag{1.32}$$

1.6 Longitudinal dipolar relaxation of two spins

A system of two spins will have four energy levels according to the following diagram.

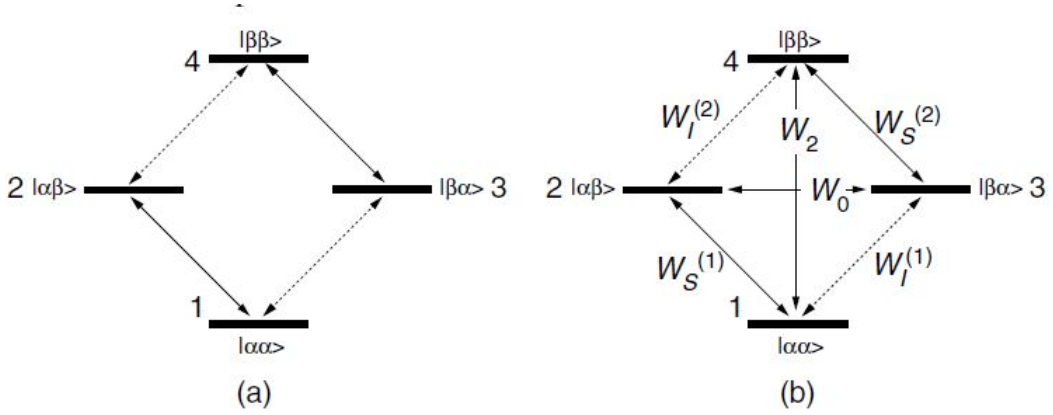

Figure 1.4: Diagram (a) shows the energy levels of a two spin system; the levels are labelled with the spin of I first and the spin of S second. The dashed and solid arrows indicate allowed transitions of the I spin and S spin respectively. Diagram (b) shows the relaxation induced transitions which are possible amongst the same set of levels.[1] Diagram adapted from[1] .

I and S spins are first and second spins. By this diagram we can write rate of change of the population of level 1 as

$$\begin{aligned}\frac{dn_1}{dt} = \quad & -W_1^{(2,\alpha)}(n_1 - n_1^0) - W_1^{(1,\alpha)}(n_1 - n_1^0) - W_2(n_1 - n_1^0) \\ & +W_1^{(2,\alpha)}(n_2 - n_2^0) + W_1^{(1,\alpha)}(n_3 - n_3^0) + W_2(n_4 - n_4^0) \end{aligned} \tag{1.33}$$

Similarly we can write equations for rate change of population of level 2,3,4 also using this diagram. Transition 1-3 and 2-4 belongs to spin one so z-magnetization of spin one is given by

$$I_{1z} = (n_1 - n_3) + (n_2 - n_4)$$

Similarly transition 1-2 and 3-4 belongs to spin two so z-magnetization of spin two is given by

$$I_{2z} = (n_1 - n_2) + (n_3 - n_4)$$

Difference between population of both spins transition is:

$$2I_{1z}I_{2z} = (n_1 - n_2) - (n_3 - n_4)$$

At equilibrium the magnetization is also defined in terms of equilibrium population:

$$I_{1z}^0 = (n_1^0 - n_3^0) + (n_2^0 - n_4^0)$$

Similar for I_{1z}^0 and equilibrium value of $2I_{1z}I_{2z}$ is zero, $2I_{1z}^0 I_{2z}^0 = 0$. After solving these equations for n_1, n_2, n_3 and n_4 rate equations for the magnetization can be written as:

$$\begin{aligned}
\frac{dI_{1z}}{dt} &= -R_z^{(1)}(I_{1z} - I_{1z}^0) - \sigma_{12}(I_{2z} - I_{2z}^0) - \triangle^{(1)} 2I_{1z}I_{2z} \\
\frac{dI_{2z}}{dt} &= -\sigma_{12}(I_{1z} - I_{1z}^0) - R_z^{(2)}(I_{2z} - I_{2z}^0) - \triangle^{(2)} 2I_{1z}I_{2z} \\
\frac{d2I_{1z}I_{2z}}{dt} &= -\triangle^{(1)}(I_{1z} - I_{1z}^0) - \triangle^{(2)}(I_{2z} - I_{2z}^0) - R_z^{(1,2)} 2I_{1z}I_{1z}
\end{aligned} \tag{1.34}$$

These new rate constant are defined in term of rate consatant of individual transition of spins:

$$\begin{aligned}
R_z^{(1)} &= W_1^{(1,\alpha)} + W_1^{(1,\beta)} + W_2 + W_0 \\
R_z^{(2)} &= W_1^{(2,\alpha)} + W_1^{(2,\beta)} + W_2 + W_0 \\
\sigma_{12} &= W_2 - W_0 \\
\triangle^{(1)} &= W_1^{(1,\alpha)} - W_1^{(1,\beta)} \\
\triangle^{(2)} &= W_1^{(2,\alpha)} - W_1^{(2,\beta)} \\
R_z^{(1,2)} &= W_1^{(1,\alpha)} + W_1^{(1,\beta)} + W_1^{(2,\alpha)} + W_1^{(2,\beta)}
\end{aligned} \tag{1.35}$$

Rate constant $R_z^{(1)}$ and $R_z^{(2)}$ are the self relaxation of spin 1 and spin 2 and σ_{12} describe the rate at which magnetization of spin one is transferred to spin two by relaxation process. This is called cross relaxation term in which z-magnetization is transferred from one spin to another spin. It is responsible for Nuclear Overhauser Effect (NOE). For dipolar relaxation between two spins rate constant $W_1^{(1,\alpha)} = W_1^{(1,\beta)}$ and $W_1^{(2,\alpha)} = W_1^{(2,\beta)}$. So both can be replaced by $W_1^{(1)}$ and $W_1^{(2)}$. Rate constant $\triangle^{(1)}$ and $\triangle^{(2)}$ will be zero. After putting these value in Eq.1.34 and this simplify equation 1.36 is called Solomon equations.

$$\begin{aligned}
\frac{dI_{1z}}{dt} &= -R_z^{(1)}(I_{1z} - I_{1z}^0) - \sigma_{12}(I_{2z} - I_{2z}^0) \\
\frac{dI_{2z}}{dt} &= -\sigma_{12}(I_{1z} - I_{1z}^0) - R_z^{(2)}(I_{2z} - I_{2z}^0) \\
\frac{d2I_{1z}I_{2z}}{dt} &= -R_z^{(1,2)} 2I_{1z}I_{1z}
\end{aligned} \tag{1.36}$$

where rate constants are given as

$$R_z^{(1)} = 2W_1^{(1)} + W_2 + W_0$$
$$R_z^{(2)} = 2W_1^{(2)} + W_2 + W_0$$
$$\sigma_{12} = W_2 - W_0$$
$$R_z^{(1,2)} = 2W_1^{(1)} + 2W_1^{(2)}$$

First relation of Eq. 1.36 describe if spin two is not at equilibrium, the rate change of the z-magnetization on spin one is affected by spin two which is proportional to the cross-relaxation rate constant, σ_{12}. If there is dipolar relaxation between two spins, this rate constant will be non-zero value. Thus, in case of cross relaxation, Z-magnetisation of spin one must be affected by z-magnetization on spin two. Cross relaxation leads to the NOE. It is the important tool for structural study by NMR. This equation is used in NOESY experiment which is useful for estimation of the distance in space which helps in structure characterization.[1]

1.7 Computational Chemistry

Theoretical chemistry can be defined as a mathematical description of chemistry. Chemical problems can be obtained with very highly accuracy using computational chemistry methods. Molecular mechanics and electronic structure theory are two broad areas which are used for computational studies. Molecular mechanics is based on classical physics and electronic structure theory based on quantum mechanics. The most basic and the most used *ab initio* electronic structure calculation is the Hartree-Fock (HF) method, in which correlated electron-electron repulsion is not specifically taken into account. Only the average of the correlated electron-electron repulsion is taken into calculation. It is the method used for ground state wave function and ground state energy determination of a quantum many body system. But it has a major drawback in that it does not account for the instantaneous correlated motion of electrons. Density function theory (DFT) is an alternate approach to electron correlation which is developed by Hohenberg and Kohn in 1964 in which ground state electronic energy completely determined by the electron density. These methods HF, DFT have not been described in the thesis, they are elaborately discussed in standard textbooks.[15,16]

Chapter 2

Relaxation and Diffusion studies of Pazufloxacin and Prulifloxacin

Our body functions because of the various biological processes that take place inside our body. These processes require membranes which differ on the basis of the constituents. These can be lipids and proteins which are contained inside these membranes. A biological membrane generally has a lipid bilayer structure which is quite efficient is providing strength to the membrane. The lipid bilayer structure also regulates the passage of large molecules and ions. The structure of the cell membrane allow them to behave as 2 dimensional liquids. Lipids and proteins can easily diffuse through these cellular membranes. Phospholipids face a huge hindrance and thus are unable to diffuse through these membrane freely. This diffusion of various biomolecules through these cellular membranes determine the speed of the various biological reactions that take place inside our body. If the membranes are not homogeneous, then the diffusion of these biomolecules are also affected. The diffusion studies of these biomolecules can be done using NMR techniques such as PFG spin echo NMR which is quite useful for mixture analysis.[17] ^{19}F NMR is used here to study fluoroquinolones.

2.1 ^{19}F NMR

Small molecules have always found a place in the development of various drugs and medicines and thus they are very important in various branches of the medicinal chemistry. Fluorine is heavily used in making various drugs and used for pharmaceutical purpose, 20-25 % of drugs contain at least one fluorine in their structure. Fluorine posses high electronegativity and it improves metabolic stability and thus

has various acidic and basic effects on a compound and so it is quite useful for biological studies. The presence of the fluorine increases protein-ligand interactions due to its structural diversity. Various structure activity studies have been shown that a drug with a trifluoro methyl group is more potent than a non fluorinated compound.

Fluorine is very useful in chemical biology as a probe of biomolecular structure, dynamics and interactions. The fluorine nucleus has a spin of $I = 1/2$, a high gyromagnetic ratio γ which makes the nucleus highly NMR sensitive, a 100 % natural isotope abundance, wide chemical shift dispersion and strong dipolar couplings, which makes it important for biological NMR studies.
Table shows the values for ^{1}H, ^{13}C, ^{19}F.

Spin System	Spin	Natural Abundance	Relative Sensitivity	Gyromagnetic Ratio(10^6 rad s^{-1} T^{-1})	NMR Frequency at 11.74T
^{1}H	1/2	99.98 %	1	267.513	500MHz
^{19}F	1/2	100 %	0.83	251.662	470.38MHz
^{13}C	1/2	1.1%	0.01	67.262	125.72MHz

2.2 Quinolones

Quinolones are a family of synthetic broad spectrum antibacterial drugs. The majority of clinically used quinolones belong to the subset of fluoroquinolones, which have a fluorine atom attached to the central ring system. Fluoroquinolones play an important role in the treatment of serous bacterial infections particularly community-acquired infections eg. hospital acquired. Use of fluoroquinolones for treating pneumonia is increasing. Fluoroquinolones are also effective against bronchitis and genito urinary infections.

Firstly, quinolone naldixic acid was used clinical purposes. It was discovered by Lesher and co-workers in 1962. Its activity against Gram nagetive bacteria and its short half life made it limited useful and later more modifications were done to improve activity against bacteria thus increasing the usefulness of fluoroquinolones. Flumequine was discovered as the first fluoroquinolone in 1973. Fluoroquinolones can be classified on the basis of their spectrum of activity as first, second, third and fourth generation.

Basic quinolone structure is given in shown in Fig. 2.1

Some reasons which make fluorine an essential parameter in medicinal chemistry.

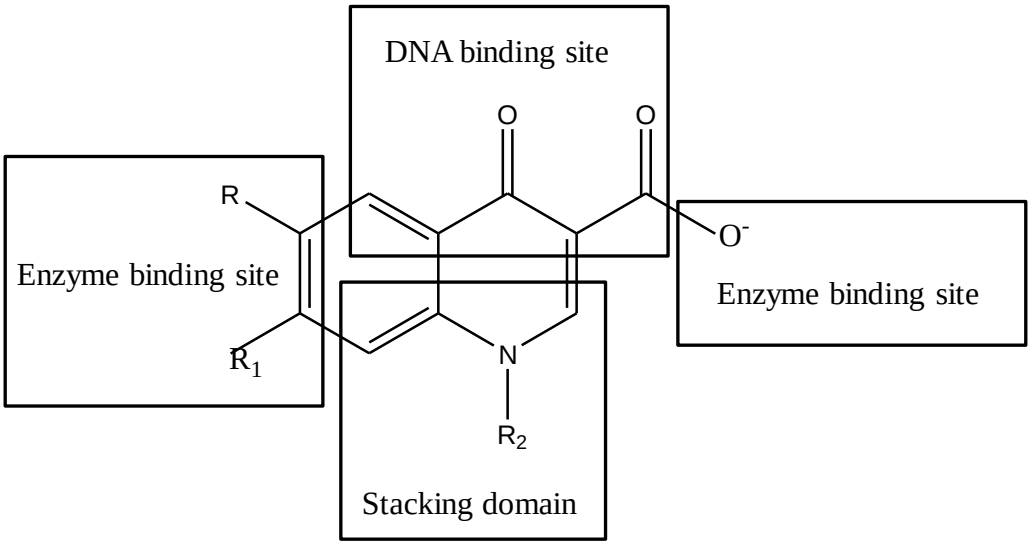

Figure 2.1: Basic quinolone nucleus structure.

Substitution of fluorine in quinolone affects their activity which are in the following way- oxo group is essential for the activity of the compound. Potency of the drug is affected by nitrogen present at ring. On the other ring, substitution at meta position (-R) results in improved antibacterial activity. Sustitution of fluorine on R_1 position improves binding affinity with DNA topoisomerase enzyme of bacteria. Carboxylic acid group binds to DNA gyrase of bacteria cell. As a result F or Cl substituent provides potentially active compound and after substitution of fluorine in quinolone, it is called fluoroquinolone, which is shown Fig. 2.2.

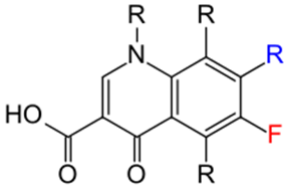

Figure 2.2: Structure of fluoroquinolone

Fluoroquinolones have a broad antibacterial spectrum of activity against gram positive and gram negative bacteria, mycobacterial pathogens and anaerobes. Fluoroquinolones act by inhibiting both DNA gyrase and topoisomerase IV enzymes thereby preventing bacterial DNA replication, transcription and repairs and recombination. The structure of fluoroquinolones reflect their pharmacological effects. Fluoroquinolones have β keto carboxylic group that is responsible for the basic pharmacological activity and acts as a binding site. The fluorine atom is responsible for cell penetration and gyrase affinity. Other substituents contribute to overall potency, antibacterial spectrum and antianaerobic spectrum.

2.2.1 Mechanism of biological action of Quinolones

Quinolones targets bacterial type II topoisomerase. Fluorine atom in quinolones is responsible for binding with bacterial DNA topoisomerase. These Quinolones and Fluroquinolones inhibits replication and transcription of bacterial DNA. Mechanism for same is given below :

During bacterial replication , Helicase is an enzyme which unwinds DNA double helix and strain in developed in DNA. DNA type II topoisomerase unwounds DNA by causing negative super-coiling of the DNA and thus relives strain o double stranded DNA. Quinolones acts on these DNA type II topoisomerase and prevent DNA from unwinding and duplicating. After binding with quinolones , DNA type II topoisomerase will not work and in this way DNA is prevented from replicating. Apart from this interaction o quinolones with (Gyrase) DNA type II topoisomerase , quinolones should also interact with DNA. This interaction is important for formation of a stable gyrase-quinolone complex essential for inhibition of bacterial replication and infection. Effectiveness of quinolone action depends on various actors like interaction with DNA, prescence of fluorine atom, stability of complexes formed, bioavailablity etc.

This chapter focuses on relaxation and diffusion studies of pazufloxacin and prulifloxacin and the interaction of two fluoroquinolones pazufloxacin and prulifloxacin with a phospholipid bilayer. Pazufloxacin is a fused tricyclic quinolone derivative with one amino cyclopropyl substituent. The presence of an amino acyl group is a unique feature that imparts broad spectrum activity against gram positive and gram negative bacteria including a variety of resistant and anaerobic bacteria. Prulifloxacin is a lipophilic prodrug, which following oral administration is rapidly observed and hydrolyzed to

the active compound ulifloxacin, which is active against gram negative and some gram positive cocii.

2.3 DPPC Lipid Bilayers

DPPC, a phospholipid containing two molecules of palmitic acid, is a pulmonary surfactant. Palmitic acid is found in plants, animals and micro-organisms as it is the most commonly available fatty acid. Phosholipids are a type of lipids which form lipid bilayers, a major component of all cell membranes. The major portion of the cell membrane of eukaryotic and prokaryotic cells is composed of lipids i.e. phospholipids. Phospholipid bilayer is composed of two polar head and a non polar hydrocarbon tail which is made up of phospholipids. The polar head, length and saturation of hydrocarbon tail determine the identity of a phospholipid. Phosopholipids play an important role in the structure and functions of a biological cell membrane[159]. Hence they should be studied in detail from every aspect. The polar head of a bilayer allows only limited number of water molecules to penetrate. ^{31}P NMR study of Pazufloxacin and Prulifloxacin with DPPC gives the information on the mobility of phosphate headgroups of DPPC.

2.4 Experimental Methods

2.4.1 Sample preparation

Pazufloxacin, Prulifloxacin and 1,2-dipaalmitoyl-sn-glycero- 3-phosphocholine (DPPC) compounds were obtained from Sigma Aldrich and were used without further purification. Samples were prepared for free diffusion in solution and for restricted diffusion inside DPPC bilayers. The samples used for free solution 1D (^1H, ^{13}C, ^{19}F), diffusion and relaxation experiments were prepared by mixing individual drugs (each having concentration 12 mM) separately in 500 μL of DMSO-d6 as solvent. For samples inserted in DPPC, required quantity of DPPC and drug were dissolved in chloroform. The solvent was evaporated with a stream of nitrogen so as to deposit a lipid film on the inner walls of the container. To remove last traces of solvent vacuum drying was used for at least 1 hour. Hydration and processing steps were performed at 50 °C, which is above the DPPC gel-fluid melting temperature (Temp = 42°C). The films were hydrated with PBS:D2O (90:10) (pH-7.4), incubated for 1 hour and sonicated for 2 hours. The lipid concentration was maintained at 50 mM and the drug

concentration was kept at 25 mM.

2.4.2 Experimental parameter

The NMR experiments were performed on the Bruker Avance III 600 MHz NMR spectrometer equipped with a 5 mm QXI probe. The standard Bruker pulse program zg30, zgpg30 and zgflqn were used to record 1D proton, ^{13}C and ^{19}F spectra respectively. Diffusion experiments were done with a single-axis actively shielded Z-gradient capable of achieving a maximum gradient strength of 53.5 Gcm^{-1}. All experiments were performed at ambient temperature (in an air-conditioned room at 22 degC). NMR data processing was done using Bruker Topspin 2.1 software. One dimensional ^{1}H, ^{13}C and ^{19}F spectra were recorded. 1D ^{1}H NMR spectra of Pazufloxacin and Prulifloxacin were obtained with 20 ppm spectral width using experimental parameters: number of scan = 16, processed with SI = 64k, TD = 132k, D1 = 1 s and line broadening (LB) = 0.3Hz. The 1D ^{19}F spectra were obtained with 5 ppm spectral width of region of interest. Experimental parameters: number of scan = 16, processed with SI = 8k, TD = 16k, D1 = 1 s and line broadening (LB) = 0.3Hz. The 1D ^{19}F spectra of the drugs inserted in DPPC were obtained with spectral width 75 ppm using experimental parameters: number of scans = 1024, and processed with SI = 2k, TD = 4 k, D1 = 2 s and LB = 0.30 Hz. The 1D ^{31}P spectra of the drug mixture in DPPC were obtained with spectral width 40 ppm using number of scans =16, processed with SI = 32 k, TD = 64 k, D1 = 5 s and LB = 1.0 Hz.

^{31}P NMR: ^{31}P NMR experiments were performed on the Bruker Avance III 400 MHz NMR spectrometer. Proton decoupled 1D ^{31}P NMR spectra were obtained using a single pulse excitation and the signal acquisition were done using WALTZ16 proton decoupling sequence.

^{1}H and ^{19}F diffusion experiment Pulse sequence "ledbpgp2s1d" was used for diffusion experiment with maximum gradient 53.5 G/cm. Experimental parameter: 16 scans, 1 ms gradient pulse (P30 = $\delta \times 0.5$), gradient recovery delay 200μ and a diffusion delay (Δ) = 50-200 ms were used for the different molecules. Experiments were done for different gradient intensity varying from 5-95% and then processing were done using Topspin 2.1 software.

2.5 Results and Discussion

Structure of Pazufloxacin and 1D ^{19}F and ^{1}H spectra are shown in Figure 2.3 and Figure 2.4.

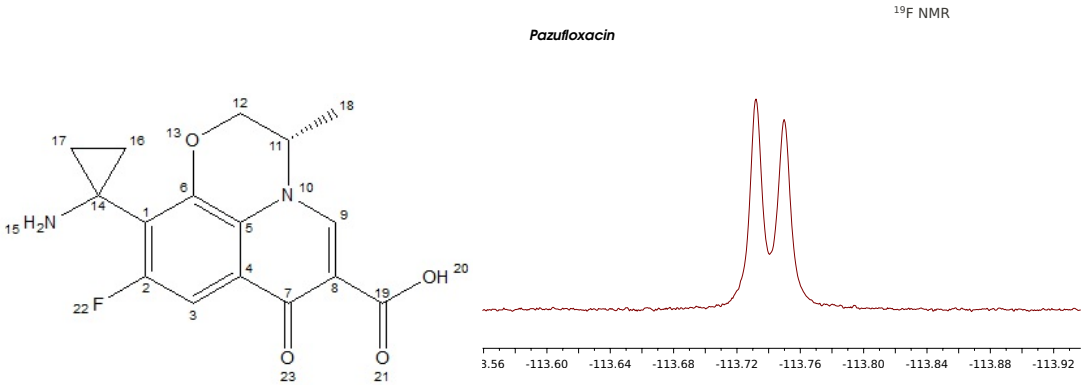

Figure 2.3: structure of Pazufloxacin and ^{19}F NMR spectra.

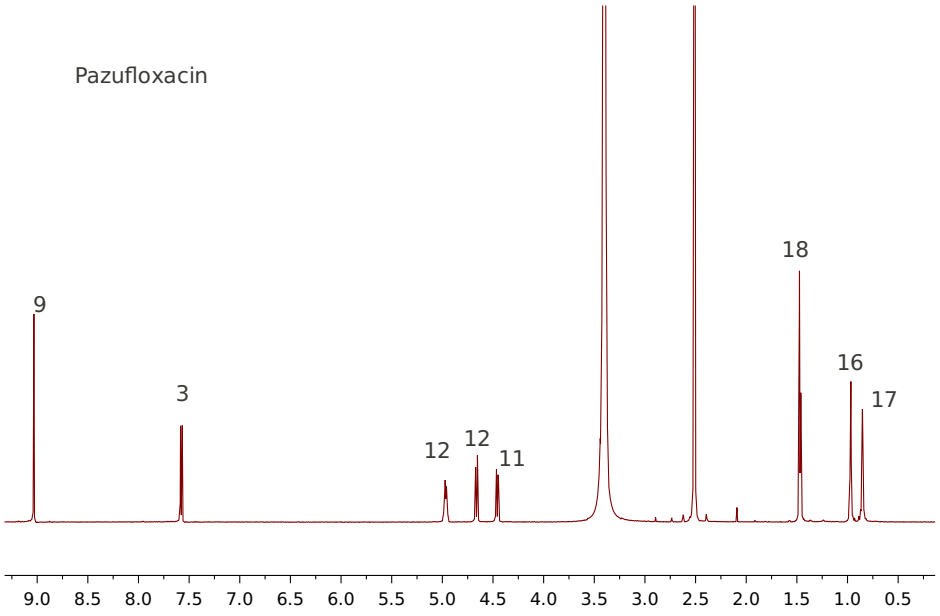

Figure 2.4: 1D ^{1}H of Pazufloxacin

The ^{1}H NMR spectra of Pazufloxacin showed signs of aromatic and non aromatic protons in the molecule. Proton attached to unsaturated carbon H9 was observed at

9.03 ppm. For the aromatic part of the ^{1}H-NMR spectra, the splitting was observed due to the presence of fluorine atom F22. The H3 proton appears as doublet at 7.5846 and 7.5679 ppm split by the fluorine atom through three bonds, with coupling constant $^{3}J_{H-F}$ = 10.01 Hz. Protons at position 18 appear as doublet at 1.4743 and 1.463 ppm splitting through three bonds. At position 12 two protons are present, both split into quartet due two bond and three bond coupling of protons. First proton at position 12 (H12) is coupled with other H12 proton with coupling constant $^{2}J_{H-H}$ = 11.6 Hz and it is also coupled with H11 with coupling constant $^{3}J_{H-H}$ = 2.21 Hz. Similarly other proton at position 12 is coupled with first proton H12 with coupling constant $^{2}J_{H-H}$ = 11.6 Hz and with H11 with coupling constant $^{3}J_{H-H}$ = 1.8 Hz. Protons at position 16 and 17 appear as triplet at 0.97 and 0.853 ppm and coupled with each other through three bonds. In ^{19}F NMR fluorine signal appears as doublet at -113.7322 and -113.750 ppm, coupled with proton (H3) through three bonds. Coupling constants $^{3}J_{H-F}$ = 10.03 Hz were found through ^{19}F NMR, which was found to be same in proton NMR.

Structure of Prulifloxacin and 1D ^{19}F are shown in Figure 2.5 and ^{1}H NMR spectra

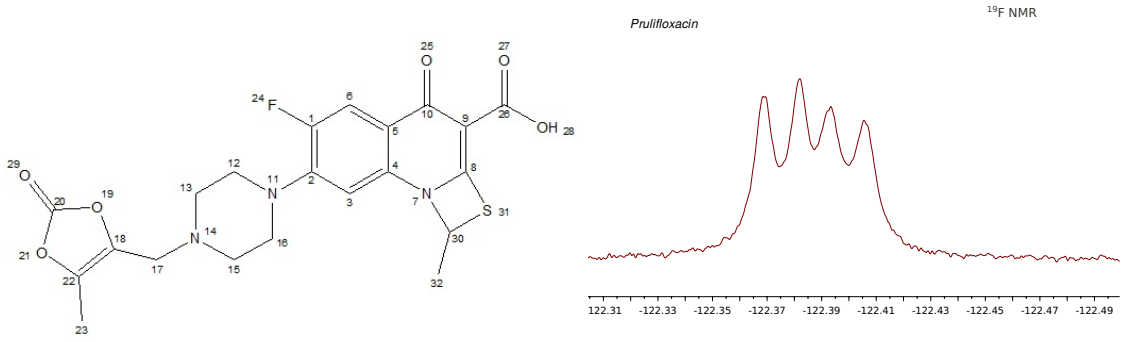

Figure 2.5: Structure and 1D ^{19}F spectra of Prulifloxacin

are shown in Figure 2.6. ^{13}C NMR is also shown for Prulifloxacin in the Figure 2.7 and chemical shift values are shown in Table 2.1. The ^{1}H NMR spectra of prulifloxacin has been assigned for aromatic and non aromatic protons in the molecules. Carboxylic proton (COOH) for prulifloxacin was observed as singlet (^{1}H) at 14.67 ppm in the spectra. For the aromatic part of the ^{1}H-NMR spectra, the characteristic splitting pattern due to the presence of fluorine atom (F24) was observed. The H6 proton in ^{1}H NMR spectra appear as doublet at 7.82 and 7.797 ppm split by the fluorine atom

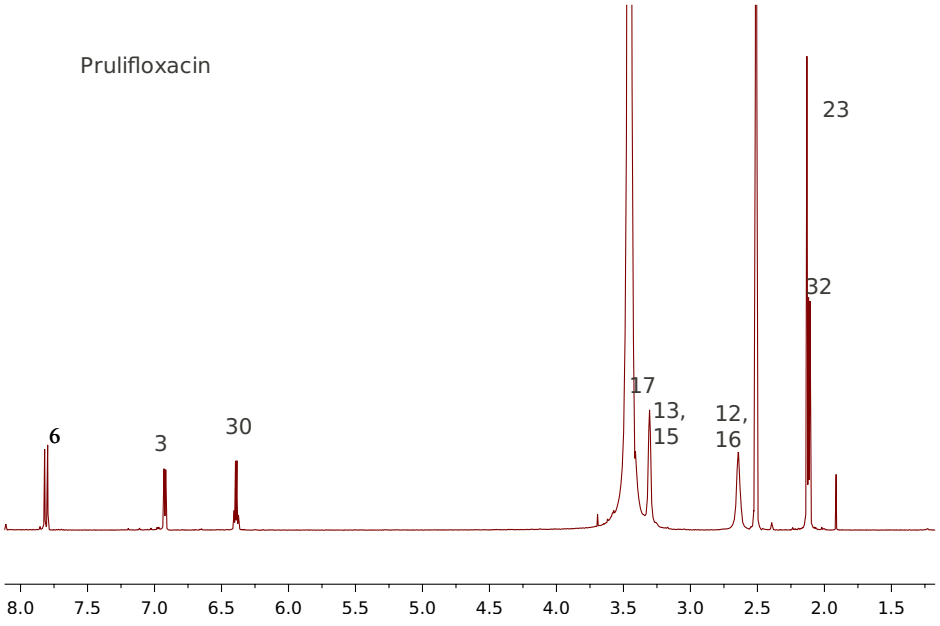

Figure 2.6: 1D ^{1}H spectra of Prulifloxacin

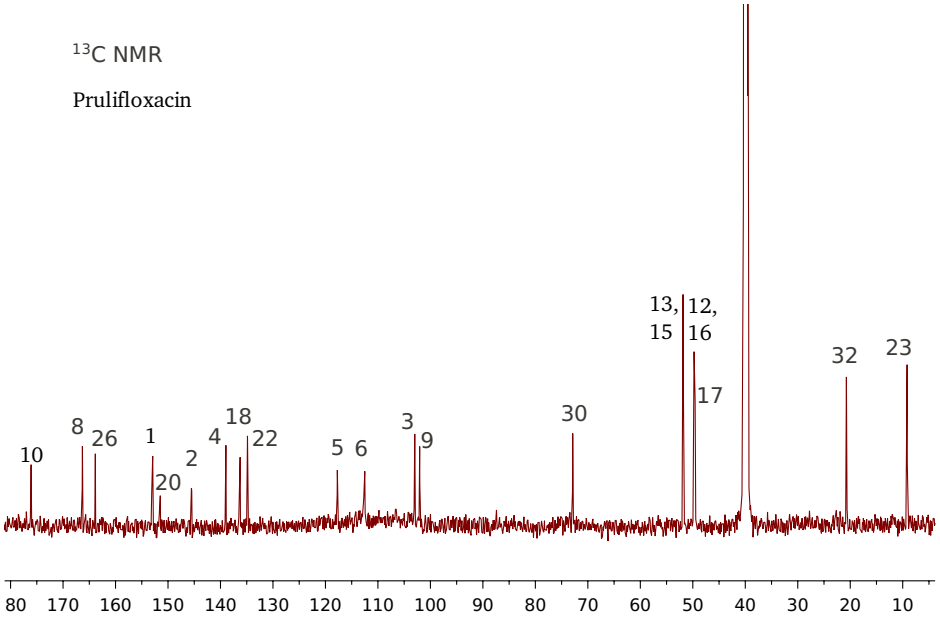

Figure 2.7: 1D ^{13}C spectra of Prulifloxacin

through three bonds, with coupling constant $^3J_{H-F}$ = 13.67 Hz. The signal of the proton H_3 appears at 6.928 and 6.916 ppm split into doublet through four bonds by the fluorine atom with coupling constant $^4J_{H-F}$= 7.27 Hz. H30 appears as quartet, being coupled with three H32 protons with coupling constant $^3J_{H-H}$= 6.3 Hz and peaks appear at 6.40, 6.395, 6.385, 6.374 ppm. Peak for H32 appear at 2.118 and 2.108 ppm as doublet and coupling constant was found $^3J_{H-H}$= 6.3 Hz. The signal for H13, H15 appear near at 3.30 ppm and for H12,H16 appear at 2.64 ppm. H13, H15 protons are coupled to H12, H16 through three bonds. H23 protons (-CH_3) appear at 2.13 ppm and H17 protons (-CH_2-) appear at 3.41 ppm in the spectrum as singlet. In ^{19}F NMR fluorine signal appears as quartet coupled with two different protons (H6, H3) through three and four bonds. Coupling constants $^3J_{H-F}$ = 13.56 Hz and $^4J_{H-F}$= 7.2 Hz were found through ^{19}F NMR. Coupling constants for $H-F$ bond were matching, estimated through both ^{19}F and ^{1}H NMR.

Proton	Chemical shift	^{13}C	Chemical shift
H28	14.67	C23	9.16
H6	7.819, 7.797	C32	20.73
H3	7.928, 7.916	C17	49.55
H30	6.406,6.395	C12,C16	49.76
	6.385,6.374	C13,C15	51.85
H32	2.118, 2.108	C30	72.88
H23	2.13	C9	102.04
H17	3.411	C3	102.04
H13,H15	3.306	C5	117.73
H12,H16	2.644	C6	112.66, 112.51
		C22	134.85
		C18	136.26
		C4	138.26
		C2	145.54, 145.48
^{19}F	Chemical shift	C1	153.08, 151.47
F24	-122.369, -122.3822	C20	152.92
	-122.3933, -122.406	C10	176.08
		C8	165.5
		C26	163.84

Table 2.1: ^{1}H, ^{13}C and ^{19}F chemical shift values (in ppm) of Prulifloxacin

The analysis of the diffusion coefficients for ^{1}H and ^{19}F from diffusion experiments for both drugs are shown in Table 2.2.

Molecule	D ^{1}H	D ^{19}F
Pazufloxacin	2.45 $\times 10^{-10} m^2/s$	2.29 $\times 10^{-10} m^2/s$
Prulifloxacin	1.94 $\times 10^{-10} m^2/s$	1.86 $\times 10^{-10} m^2/s$

Table 2.2: Diffusion coefficients (D) of prulifloxacin and pazufloxacin extracted from 1D ^{1}H and ^{19}F diffusion experiments.

Experimental analysis of drug molecule with DPPC and without DPPC gives the information of binding. Both Prulifloxacin and Pazufloxacin contain proton and fluorine groups so that their diffusion study in the DPPC lipid membrane can be done using ^{1}H and ^{19}F NMR. 1D diffusion ^{1}H NMR, ^{19}F NMR experiments of drugs, DPPC and drugs with DPPC were done. NMR signal was observed broader than pure form of drugs and broadening of the signals arise due to the exchange at an intermediate time scale between the bound and free form. The T_1 and T_2 relaxation times are measure of the overall tumbling and segmental motions in the molecule and were determined. The diffusion coefficients and T_1 and T_2 of Prulifloxacin and Pazufloxacin with DPPC are given in Table 2.3. T_2 can be estimated from NMR line width and after binding with DPPC the T_2 values come the order of 10-100 ms. Lower values of T_2 indicate that the both drugs lose their mobility and bind to lipid membrane, resulting in a loss of motional freedom.

Table 2.3: Relaxation rates and Diffusion coefficients D ($\times 10^{-11} m^2/s$) of Prulifloxacin and Pazufloxacin inside DPPC obtained from relaxation and 1D ^{1}H, 1D ^{19}F and 1D ^{31}P diffusion experiments.

Drug	Nuclei	T_1	T_2	Diffusion coefficient
Prulifloxacin with DPPC	^{1}H	1.49 s	0.78 s	1.17 ± 0.02
	^{19}F	1.34 s	0.79 s	1.20 ± 0.01
Pazufloxacin with DPPC	^{1}H	1.79 s	0.17 s	1.52 ± 0.03
	^{19}F	1.36 s	0.15 s	1.54 ± 0.01
DPPC	^{31}P	2.85 s	0.15 s	1.62 ± 0.02
	^{1}H	1.95 s	0.68 s	1.60 ± 0.03

2.6 Measurement of Relaxation Times

The phenomena of longitudinal and transverse relaxation time constants were given by Bloch.[18,19] Methods used for T_1 and T_2 determination are described in the following subsections.

2.6.1 Determination of T_1

There are several methods that exist for T_1 determination.[6,20] Here constant T_1 was determined by the inversion recovery method.[21,22] The pulse sequence for inversion recovery method is shown in Figure 2.8 using nonselective rf pulses. Experiments were performed for variable delays and τ delay vs. signal intensity data was fitted in GNUPLOT using Eq. 2.2

Inversion recovery technique is used to measure T_1. In this experiment, pulse sequence consists of two RF pulse separated by an interval τ. The pulse sequence is repeated with different values of the interval τ. For each value of τ, we repeat the pulse sequence and acquire the data number of times. Each repetition of the pulse sequence is separated by a long interval τ_{wait}, so that spins can return to thermal equilibrium state. The sequence starts with 180^0 pulse that invert the population to -Z

$$M(0) = M_0 \xrightarrow{180^0} -M_0 \tag{2.1}$$

and then 90^0 pulse gives after the delay time τ, that delay time allow to relax the spins. After the 90^0 pulse magnetization appears in transverse plane and FID is acquired. The build up magnetization is given by

$$M_z = M_0(1 - 2exp(-t/T_1)) \tag{2.2}$$

Pulse sequence for Inversion Recovery Experiment is shown in Fig. 2.8.

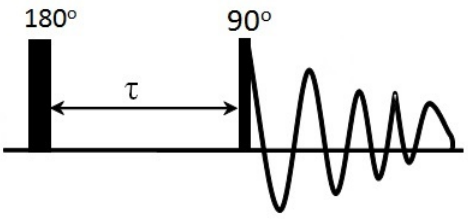

Figure 2.8: Inversion recovery experiment

The fitted plots of τ delay vs. signal intensity are shown in the Figure 2.9. For good estimation of the T_1 values large number of measurements were taken.

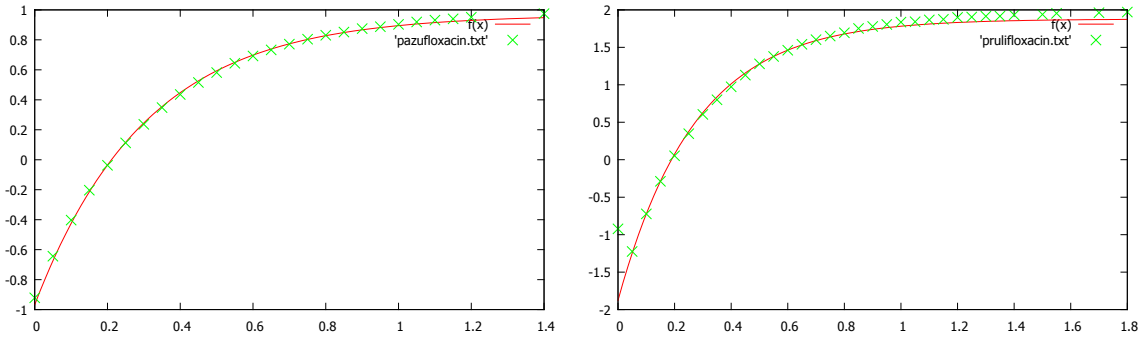

Figure 2.9: ^{19}F T_1 determination of Pazufloxacin and Prulifloxacin using inversion recovery experiment.

2.6.2 Determination of T_2

The T_2 constant was determined by CPMG spin-echo method. Ploting and calculation for T_2 was done using GNUPLOT software.

Spin Echoes

The method using strong rf field was first given by Erwin Hahn[23] and he was the one who introduced the spin echo sequence.[24] The pulse sequence for spin echo there is given in Figure 2.10

The Hahn echo pulse sequence consists of two RF pulse. Firstly, there is an initial excitation $(\pi/2)_x$ pulse, which is followed by another $(\pi/2)_x$ pulse after a time interval $\tau/2$. The signal will disappear before applying the second $(\pi/2)_x$ pulse ($T_2 \leq \tau/2$). It

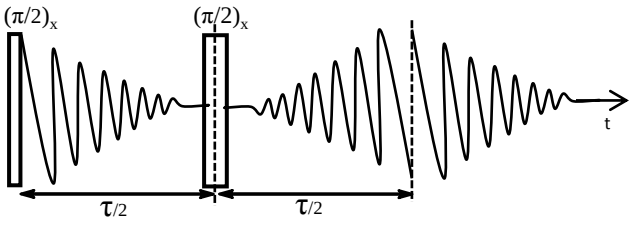

Figure 2.10: The Hahn spin echo pulse sequence.

will reappear again at time t = τ. This creates echoes, hence the name of the sequence.

The principle of the Hahn echo is shown in Figure. 2.11.[2,24] First $(\pi/2)_x$ pulse flips the longitudinal magnetization into the transverse plane (x,y) (1). Then spins start unwinding due to the variation in the magnetic field in the sample which causes local field inhomogeneities. So dephasing of spins make the signal decay (2). After applying the second $(\pi/2)_x$ at time t = $\tau/2$, x-component of the transverse magnetization is not affected (3) but the y-component is flipped back to z-axis (4). X-component of the spins will precess during the second interval time $\tau/2$ and create the echo (5). If the third pulse is applied during the time $\tau \leq T_2$, z-component is flipped back to transverse plane again (6) and it creates a stimulated echo at time T+ τ (7).

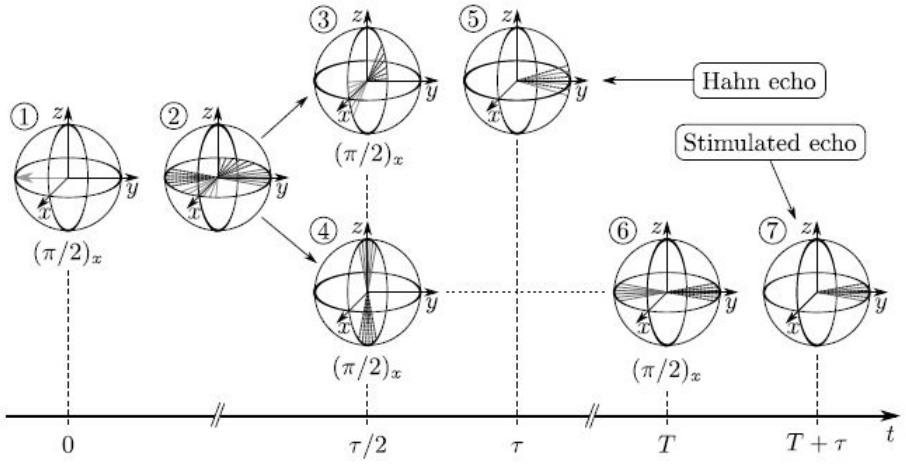

Figure 2.11: Hahn and stimulated spin echoes. Adapted from[2]

In Hahn echo method only one component of the transverse magnetization is responsible for echo. It was not so much of a successful technique to use. To improve the method a partial modification was done by Carr-Purcell (CP)[25] Two versions of the CP echoes were published, which is shown in Figure 2.12.

"Method A" is just simple extension of original Hahn echo method. In this method π_x is used instead of second $(\pi/2)_x$ pulse, by which complete refocussing of the magnetization was allowed. To calculate T_2 value, for different τ values the sequence was repeated. If the B_0 inhomogeneity and diffusion are significant and for long T_1 values, Method A becomes less efficient. To calculate the T_2 values instead of one π_x pulse, large number of π_x pulse are used continuously. So by using "Method B" repeated refocusing and multiple spin echo signals can be obtained in one scan.

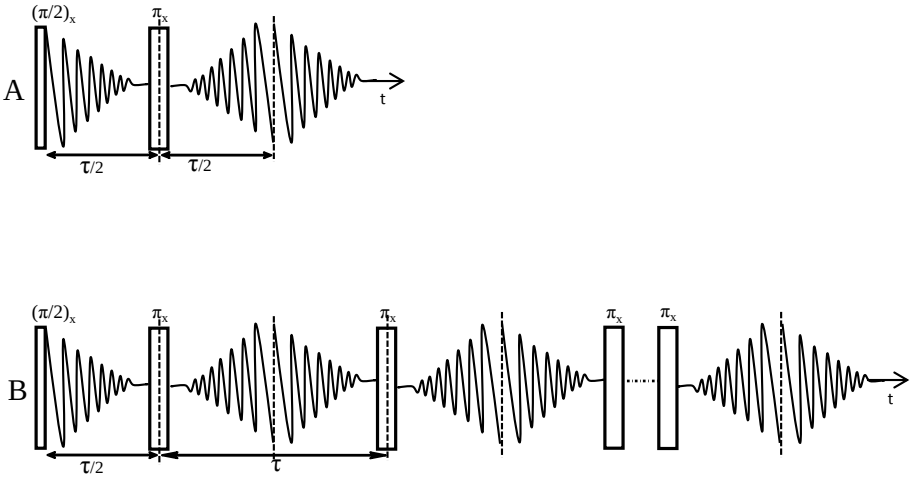

Figure 2.12: The CP spin echo pulse sequence

Comparison between Method A and Method B depends on the refocusing accuracy of the π pulse because if length of π pulse is not accurate, the flip angle will be different from 180^0. Spin echoes are used in J-spectroscopy[26] and for polarization transfer between coupled nuclear spins (INEPT).[2] In solid-state NMR due to dipolar and quadrupolar interactions, an alternative of the Hahn echo, solid echoes are used.[27]

CPMG Spin Echo sequence

In this pulse sequence, initially z-magnetization is flipped towards x-axis by appling $(\pi/2)_y$ pulse. Before applying second pulse $\tau/2$ delay is given and during this interval spins are allowed to freely evolve. Spins start unwinding due to the variation in the magnetic field in the sample which causes local field inhomogeneities. So dephasing of spins make the signal decay and π_x is applied after the delay which causes refocusing of the spins at time t = $\tau/2$ after second pulse.[28] Transverse magnetization is given by:

$$M_{xy}(t) = M_{xy}exp(-t/T_2) \tag{2.3}$$

Pulse sequence of CPMG spin echo is given in the following figure.

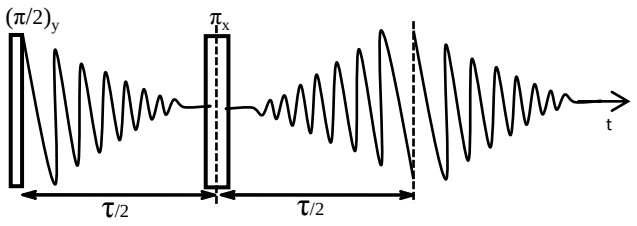

Figure 2.13: The CPMG spin-echo sequence.

2.7 Conclusion

We performed experiments on Prulifloxicin and Pazufloxacin with and without using DPPC and did the analysis for them. Diffusion experiment can be used to differentiate similar molecular mass compounds by characterizing their diffusion coefficients. This analysis gives us information about the binding of fluorinated drugs to DPPC lipid bilayer. Lowering of diffusion coefficient values of these drugs evidently showed that these drugs bind to DPPC. Binding of drugs with DPPC led to line broadening which is a direct measure of T_2. With the increase of line broadening, the value of T_2 decreases and this decrease in the value of T_2 means a loss in the mobility of drugs and thus leads to an increase in the number of bindings to lipid membrane. This study is useful in future as any new drug can be developed and binding studies can help in modification in steric configuration of drug for effective drug action.

Chapter 3

Experimental analysis of Fluoroquinolones

This chapter focuses on the experimental methods of fluoroquinolones. It includes 1D and 2D experiments and their relaxation study. There are few quinolones which are studied here. They are Difloxacin, Pefloxacin, Levofloxacin, Flumequine, Fleroxacin and Trovafloxacin. Difloxacin has two fluorine at two different rings in which one fluorine is coupled to two protons and other fluorine is coupled to four protons, resulting in multiplet spectra for fluorine. Pefloxacin has one fluorine coupled to two inequivalent protons and its fluorine spectra gives quartet. Levofloxacin has one proton coupled to one fluorine. Flumequine has two equivalent protons coupled to fluorine. Fleroxacin has two fluorine at different rings and both fluorines are attached to two protons individually. Trovafloxacin has three fluorines, two fluorines are on same ring and one fluorine is on other ring, coupled to the one proton.

3.1 Experimental methods

Fluoroquinolones were purchased from Sigma-Aldrich and were used without any further purification. Sample of these fluorinated drugs were prepared by adding 5mM of the sample in 500μL of DMSO or D_2O solvent.
The NMR experiments were performed on the Bruker Avance III 600 MHz NMR spectrometer equipped with a 5 mm QXI probe. The standard Bruker pulse program zg30, zgpg30 and zgflqn were used to record 1D proton, ^{13}C and ^{19}F spectra respectively. Diffusion experiments were done with a single-axis actively shielded Z-gradient capable of achieving a maximum gradient strength of 53.5 Gcm^{-1}. All experiments

were performed at ambient temperature (in an air-conditioned room at 22 degC). NMR data processing was done using Bruker Topspin 2.1 software. One dimensional ^{1}H, ^{13}C and ^{19}F spectra were recorded. 1D ^{1}H NMR spectra of fluoroquinolnes were obtained with 20 ppm spectral width using experimental parameters: number of scan = 16, processed with SI = 64k, TD = 132k, D1 = 1 s and line broadening (LB) = 0.3Hz. The 1D ^{19}F spectra were obtained with 5 ppm spectral width of region of interest. Experimental parameters: number of scan = 16, processed with SI = 8k, TD = 16k, D1 = 1 s and line broadening (LB) = 0.3Hz. Relaxation experiments for ^{1}H and ^{19}F were done using t1ir1d and cpmg1d pulse sequences for longitudinal and transverse relaxation. For ^{13}C relaxation, experiments were obtained with 238 ppm spectral width using t1ir1dpg pulse sequence. Experimental parameters: number of scan = 1024, processed with SI = 132k, TD = 64k and line broadening (LB) = 7 Hz. T_1 and T_2 time constants were calculated using GNUPLOT software.

3.2 1D experiments

1D experiments for ^{1}H, ^{13}C and ^{19}F were done for all five fluorinated drugs. Their spectra and peak assignment are shown in the respective figures. Peak in each ^{1}H spectra is observed at 2.5 ppm as pentet is due to the DMSO solvent. One more peak, that of water appears at 3.3 ppm due to DMSO solvent.

The ^{1}H and ^{13}C NMR spectra of Difloxacin showed signs for aromatic and non

^{13}C	Chemical shift	^{13}C	Chemical shift
C25	42.38	C12,C16	130.44
C20, C24	46.51	C11	136.59
C21, C23	52.24	C4	139.51
C3	107.62	C2	144.43
C9	107.98	C1	149.52
C6	111.87	C14	152.53
C13,C15	117.85	C26	166.15
C5	119.94	C10	177.22

Table 3.1: ^{13}C chemical shift values (in ppm) for Difloxacin

aromatic protons in the molecule. Carboxylic proton (COOH) for Difloxacin was observed as singlet (^{1}H) at 15.05 ppm in the spectra. Proton attached to unsaturated carbon H30 was observed at 8.69 ppm. For the aromatic part of the ^{1}H-NMR

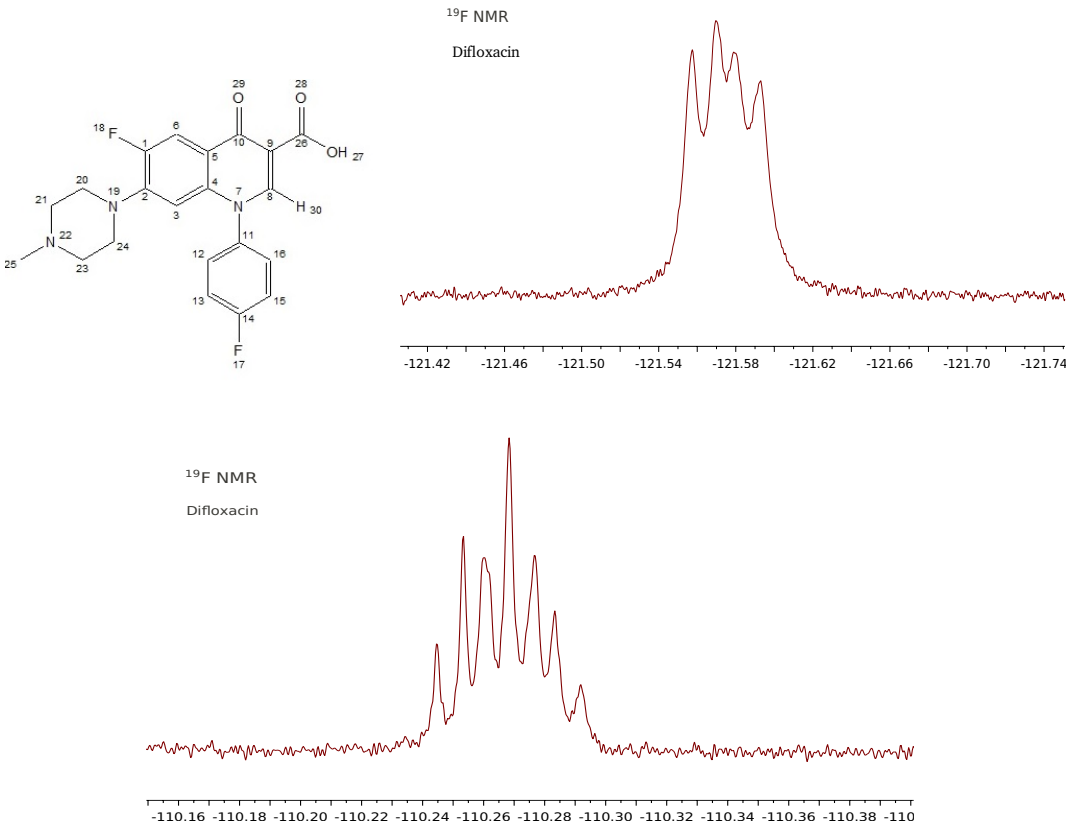

Figure 3.1: Structure and 1D ^{19}F spectra of Difloxacin

spectra, the characteristic splitting pattern due to the presence of fluorine atom (F17 and F18) was observed. The H6 proton in ^{1}H NMR spectra appears as a doublet at 8.085 and 8.064 ppm split by the fluorine atom through three bonds, with coupling constant $^{3}J_{H-F}$ = 12.78 Hz. The signal of the proton H_3 appears at 6.446 and 6.434 ppm split into doublet through four bonds by the fluorine atom with coupling constant $^{4}J_{H-F}$= 7.22 Hz. The signal for H13, H15 appear as quartet split by fluorine and nearby proton atoms (H12, H16 respectively) through three bond, with coupling constant $^{3}J_{H-F}$ = 9.4 Hz and $^{3}J_{H-H}$ = 6.74 Hz. H12, H16 also split by fluorine through four bond and nearby protons (H13, H15 respectively) through three bond, with coupling constant $^{4}J_{H-F}$ = 6.8 Hz and $^{3}J_{H-H}$ = 6.8 Hz and signal appears as quartet. Similarly H20, H24 are coupled to H21, H23 respectively through three bonds and give multiplet pattern in ^{1}H spectra. H25 protons appear as singlet at 2.792 ppm.

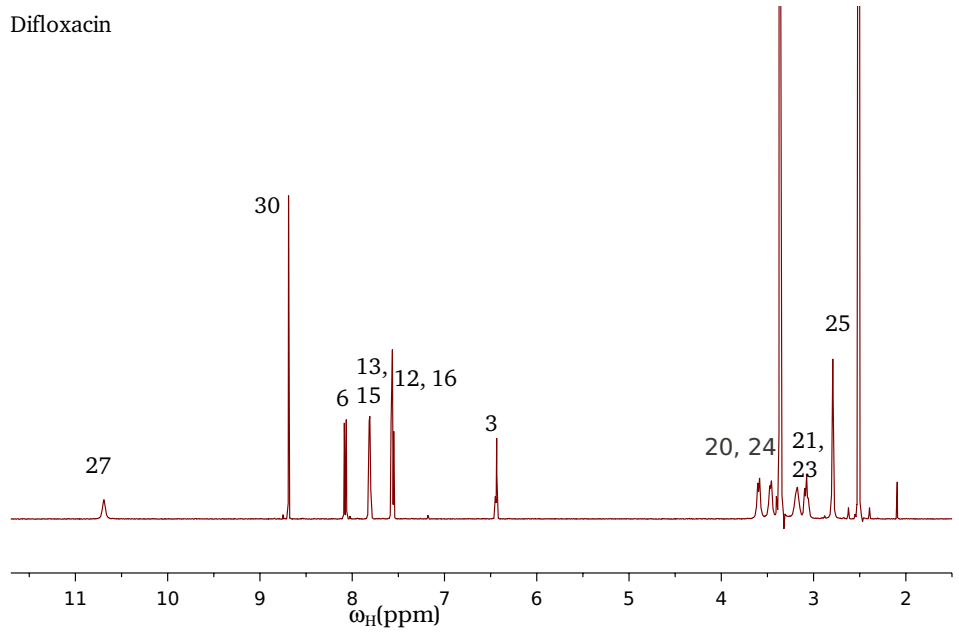

Figure 3.2: 1D ^{1}H spectra of Difloxacin

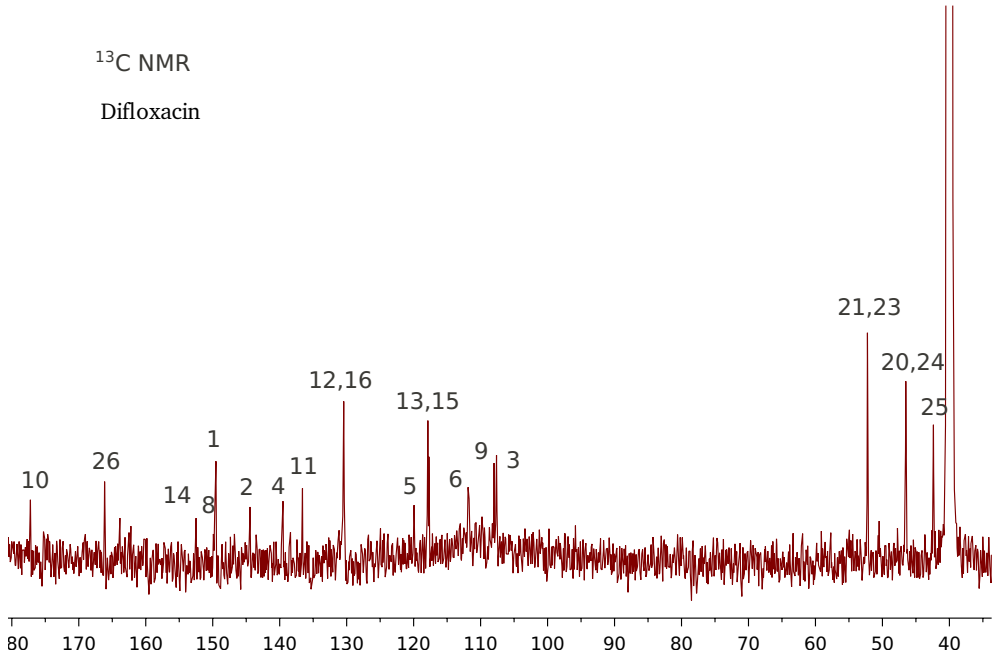

Figure 3.3: 1D ^{13}C spectra of Difloxacin

The ^{1}H and ^{13}C NMR spectra of Flumequine showed for aromatic and non aromatic protons in the molecule. Carboxylic proton (COOH) (H17) was observed as singlet

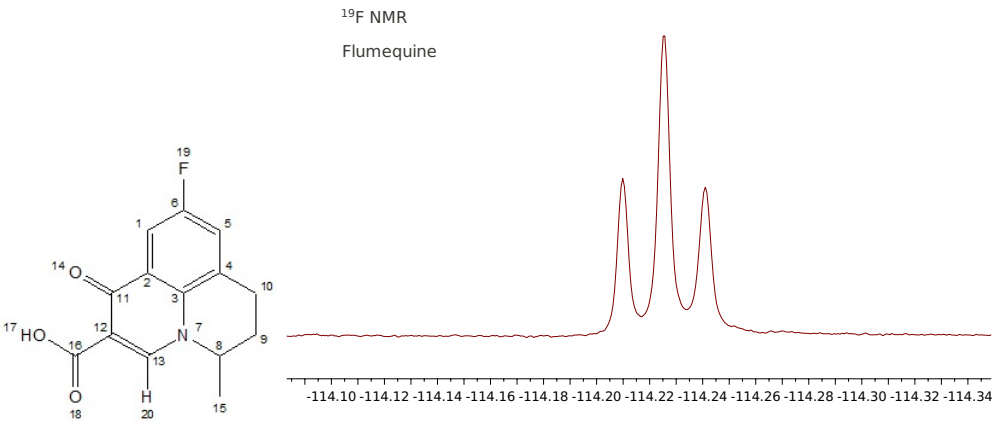

Figure 3.4: Structure and 1D ^{19}F spectra of Flumequine

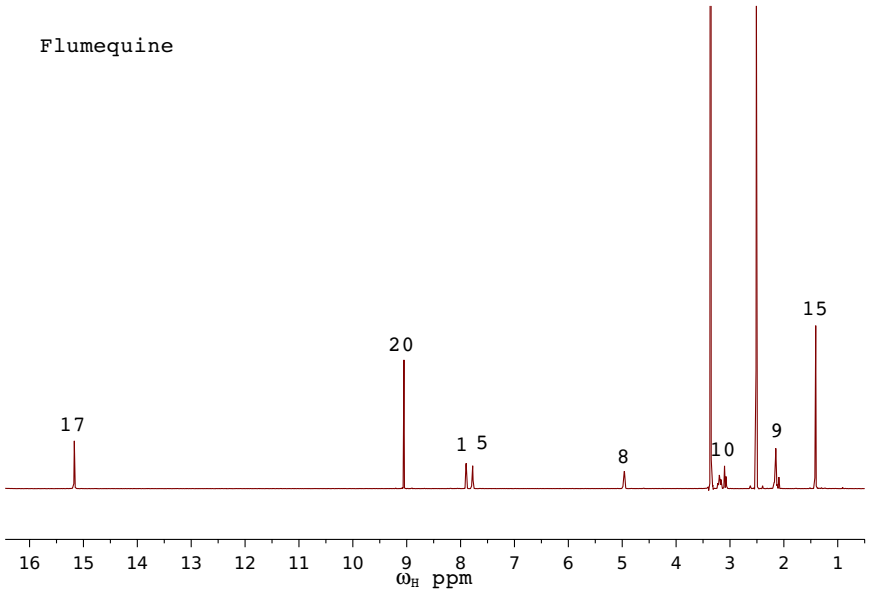

Figure 3.5: 1D ^{1}H spectra of Flumequine

(^{1}H) at 15.17 ppm in the spectra. Proton attached to unsaturated carbon (H20) was observed at 9.05 ppm. For the aromatic part of the ^{1}H-NMR spectra, the char-

acteristic splitting pattern due to the presence of fluorine atom F19 was observed. The H1 proton appears as quartet at 7.901, 7.896, 7.8866 and 7.882 ppm split by the fluorine atom through three bonds and proton (H5) through four bonds, with coupling constant $^{3}J_{H-F} = 8.8$ Hz and $^{4}J_{H-H} = 2.96$ Hz. Same pattern appears for H5 proton due to coupling with fluorine and proton (H1) and coupling constants are $^{3}J_{H-F} = 9$ Hz and $^{4}J_{H-H} = 2.96$ Hz. H8 appears as a multiplet and near is to 4.96 ppm due to three bond couplings with two (H9) protons and three (H15) protons. H10 gives the triplet signal at 3.10 ppm split due to two H9 protons. H9 protons signal appear as multiplet and near to 2.149 due to coupling with H8 and two H10 protons. There are three protons attached to the C15 and these protons appear as doublet through three bond (H15-H8) with coupling constant $^{3}J_{H-H} = 6.83$ Hz. As shown in ^{13}C NMR Spectra C6 peak split into doublet with one bond coupling constant $^{1}J_{C-F}$= 246.94 Hz. C1 and C5 also appear as a doublet through two bonds with coupling constants $^{2}J_{C-F}$= 23.29 Hz and 25.43 Hz.

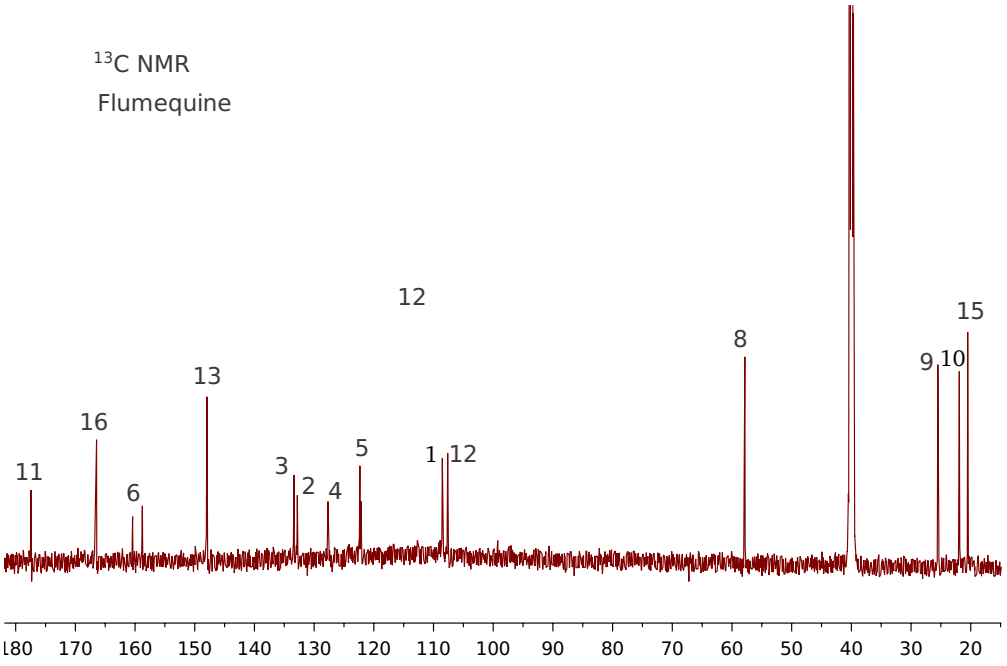

Figure 3.6: 1D ^{13}C spectra of Flumequine

^{13}C	Chemical shift	^{13}C	Chemical shift
C15	20.51	C4	127.684
C10	21.91	C2	132.81
C9	25.51	C3	133.81
C8	57.84	C13	147.96
C12	107.62	C6	160.42, 158.78
C1	108.52, 108.37	C16	166.45
C5	122.33, 122.16	C11	177.42

Table 3.2: ^{13}C chemical shift values (in ppm) for Flumequine.

The ^{1}H NMR spectra of Fleroxacin showed for aromatic and non aromatic protons in the molecule. Carboxylic proton (COOH) was observed as singlet (^{1}H) at 14.86

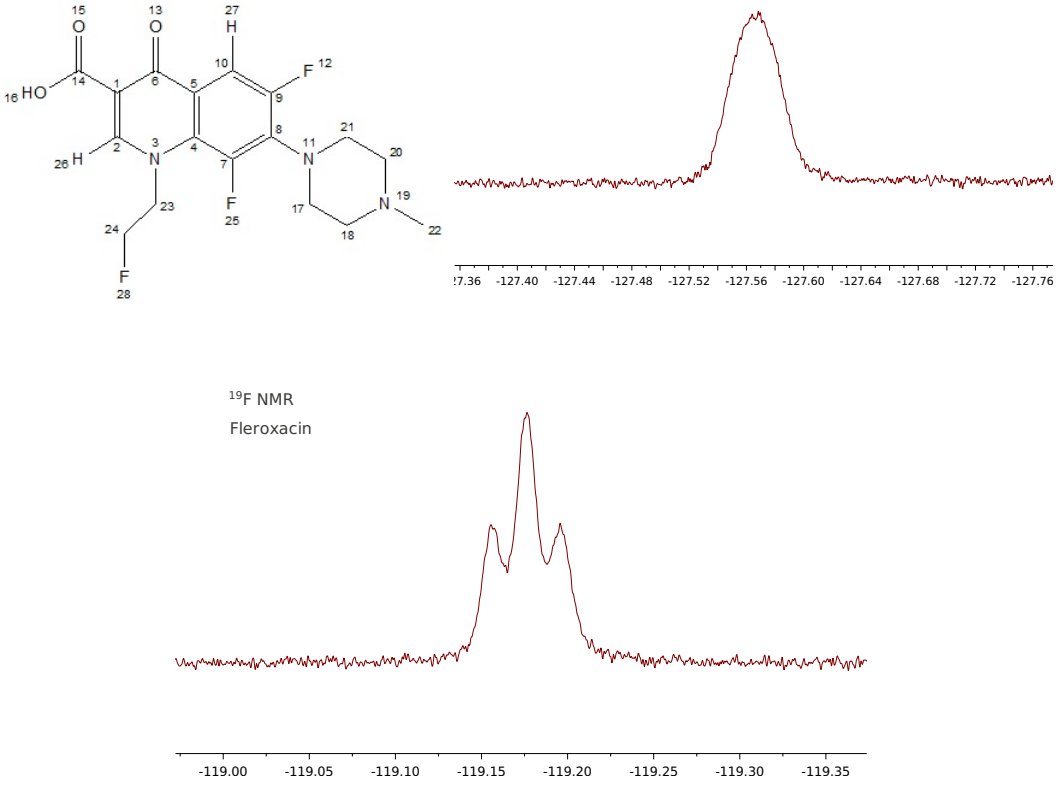

Figure 3.7: structure and 1D ^{19}F spectra of fleroxacin

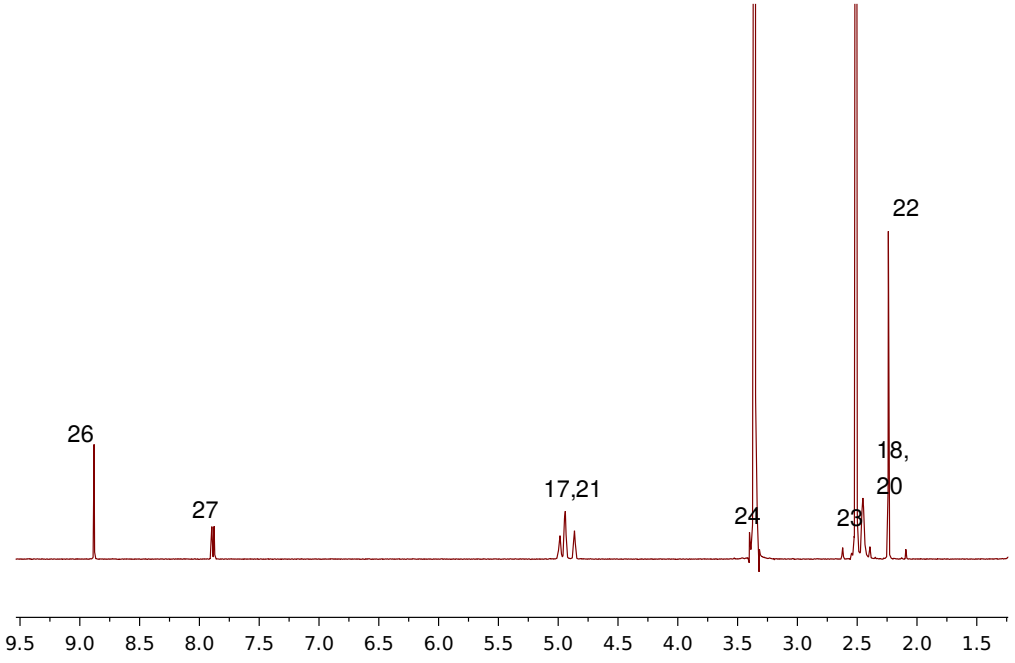

Figure 3.8: 1D ^{1}H spectra of Fleroxacin

ppm in the spectra. Proton attached to unsaturated carbon H26 was observed at 8.88 ppm. In the aromatic part of the ^{1}H-NMR spectra, proton H27 was observed as a doublet through three bond coupling with fluorine F12, with coupling constant $^{3}J_{H-F}$ = 11.58 Hz. There was no splitting observed due to the F25 in the proton H27 signal. The signal for H17, H21 appear as triplet split by two nearby protons attached to each carbon C18, C20 (H18, H20) respectively, coupled through three bond coupling and vice-versa H18, H20 also appear as triplet due to coupling with H17, H21 protons respectively. Two H24 protons appear as multiplet due to three bond coupling with two protons (H23) and two bond coupling with fluorine (F28). There are three protons attached to the C15 (-CH_3), appear as singlet at 2.24 ppm.

The ^{1}H NMR and ^{13}C spectra of Levofloxacin showed signed for aromatic and non aromatic protons in the molecule. Carboxylic proton (COOH) was observed as singlet (^{1}H) at 15.24 ppm in the spectra. Proton attached to unsaturated carbon H28 was observed at 8.98 ppm. For the aromatic part of the ^{1}H-NMR spectra, the splitting was observed due to the presence of fluorine atom F12. The H3 proton appears as doublet at 7.598 and 7.578 ppm split by the fluorine atom through three bonds, with

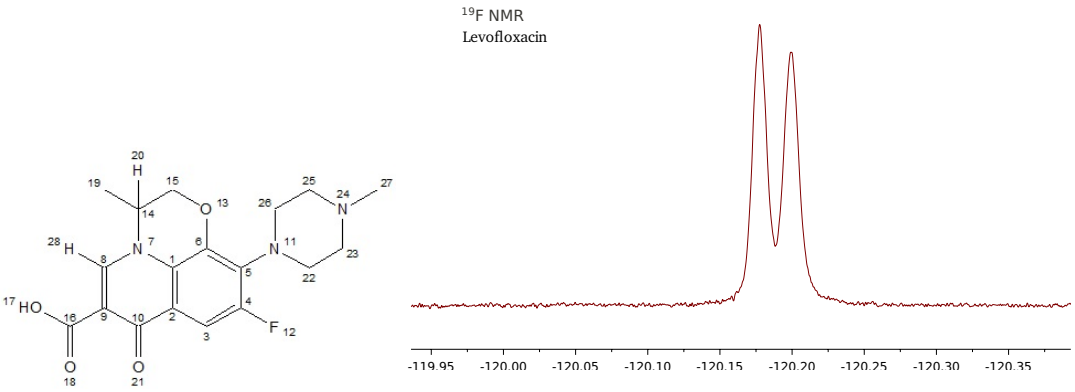

Figure 3.9: structure and 1D ^{19}F spectra of Levofloxacin

^{13}C	Chemical shift	^{13}C	Chemical shift
C19	18.38	C2	119.91, 119.97
C27	46.50	C1	125.17
C26, C22	50.52	C5	132.53, 132.43
C14	55.26	C8	146.52
C25, C23	55.72	C6	140.48
C15	68.46	C4	156.64, 155.01
C3	103.74, 103.59	C16	166.48
C9	107.1	C10	176.72

Table 3.3: ^{13}C chemical shift values (in ppm) for Levofloxacin

coupling constant $^{3}J_{H-F} = 12.33$ Hz. Proton H20 appears as multiplet near 4.92 ppm splitting due to three bond coupling with H15 and three H19 protons. At position 15 two protons are present, both split into quartet due to coupling with two bond and three bond coupling of protons. First proton at position 15 (H15) coupled with other H15 proton with coupling constant $^{2}J_{H-H} = 11.4$ Hz and also coupled with H20 with coupling constant $^{3}J_{H-H} = 1.5$ Hz. Similarly other proton at position 15 is coupled with first proton H15 with coupling constant $^{2}J_{H-H} = 11.4$ Hz and also coupled with H20 with coupling constant $^{3}J_{H-H} = 2.2$ Hz. The signal for H22, H26 appear as triplet near at 3.31 and 3.29 ppm split by nearby protons H23, H25 respectively. H23, H25 also split into triplet near 2.4 ppm, by nearby protons H22, H26 respectively through three bond. Protons at position 27 appear as singlet at 2.234 ppm. Signal for H19 protons split into doublet at 1.454 and 1.44 ppm due to three bond coupling

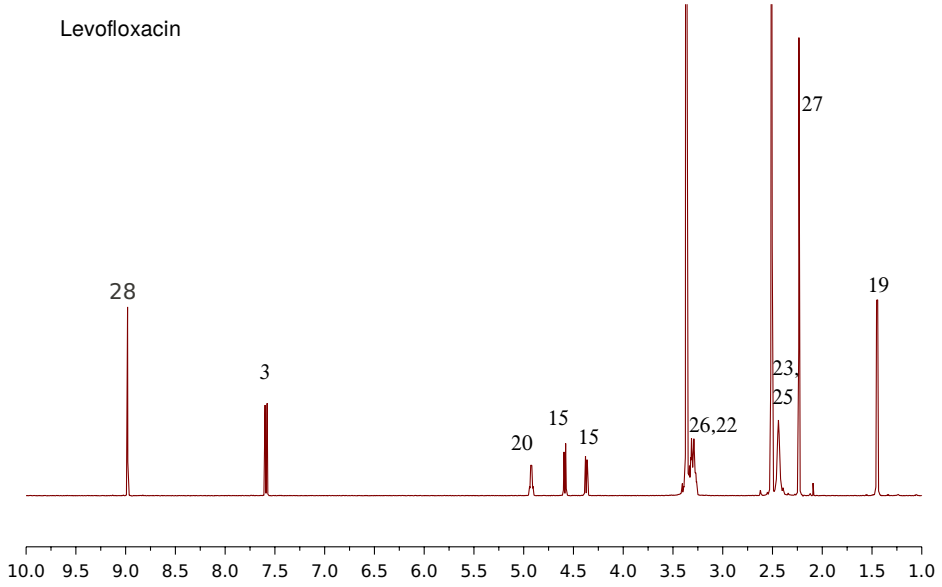

Figure 3.10: 1D ^{1}H spectra of Levofloxacin

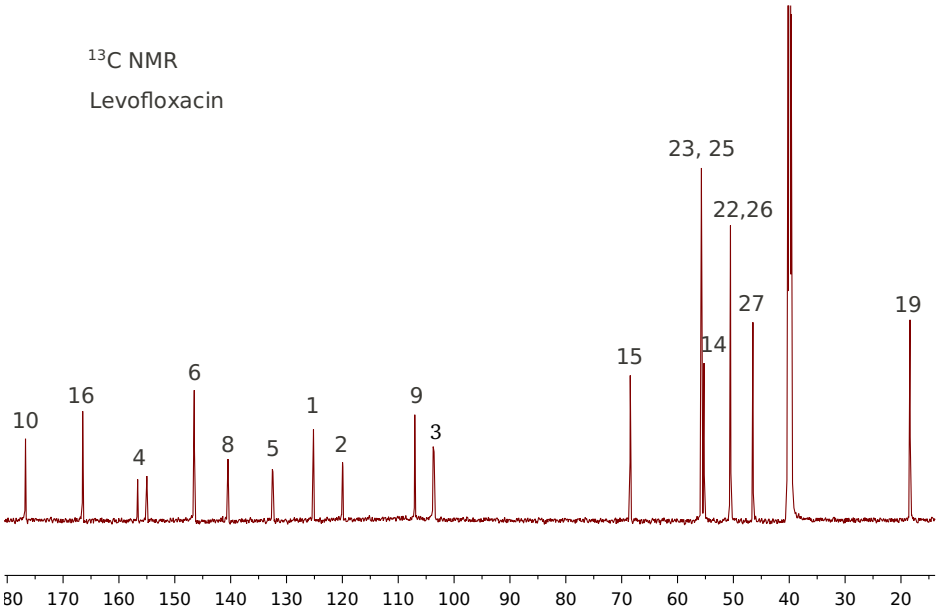

Figure 3.11: 1D ^{13}C spectra of Levofloxacin

with H20 and coupling constant was $^{3}J_{H-H} = 6.7$ HZ. As shown in ^{13}C NMR Spectra C4 peak split into doublet with one bond coupling constant $^{1}J_{C-F}$= 243.4 Hz. C3

and C5 also appear as a doublet through two bonds with coupling constants $^{2}J_{C-F}$= 23.38 Hz and 13.97 Hz.

The ^{1}H NMR and ^{13}C spectra of Pefloxacin showed signs of for aromatic and

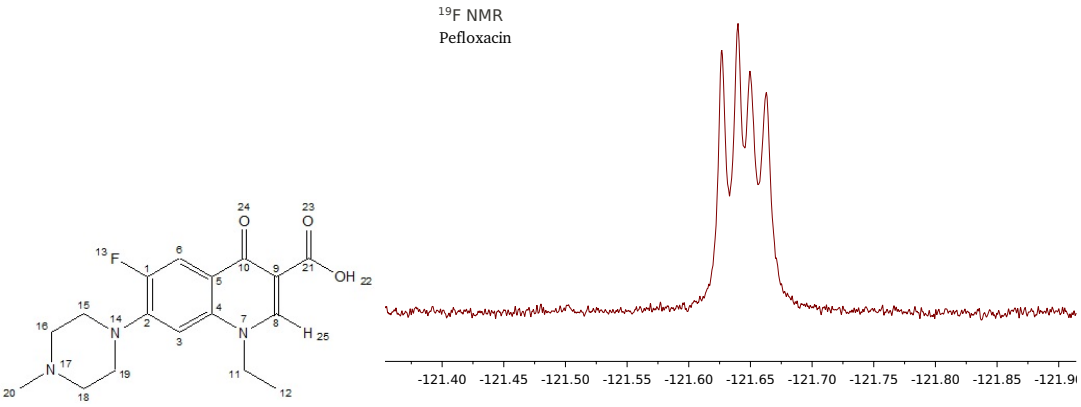

Figure 3.12: structure 1D ^{19}F spectra of Pefloxacin

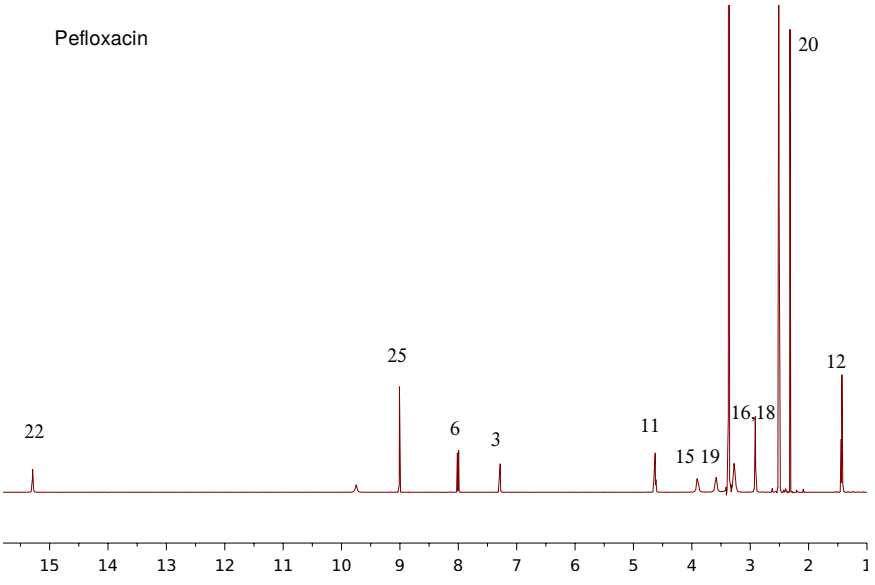

Figure 3.13: 1D ^{1}H spectra of Pefloxacin

non aromatic protons in the molecule. Carboxylic proton (COOH) was observed as

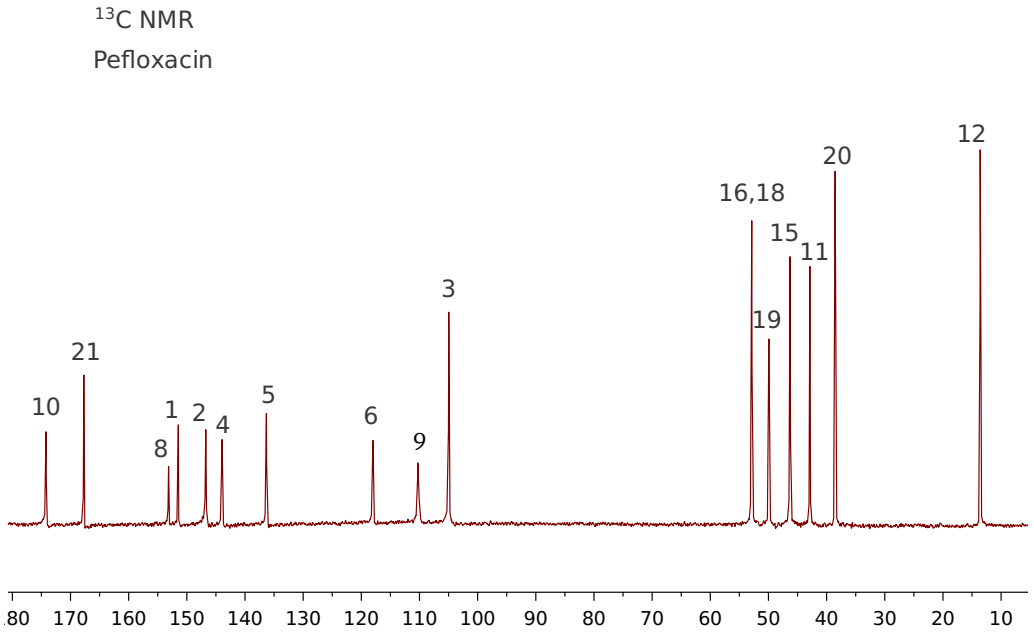

Figure 3.14: 1D ^{13}C spectra of Pefloxacin

singlet (^{1}H) at 15.29 ppm in the spectra. Proton attached to unsaturated carbon H29 was observed at 9.01 ppm. For the aromatic part of the ^{1}H-NMR spectra, the splitting was observed due to the presence of fluorine atom F13. The H6 proton appears as doublet at 8.015 and 7.994 ppm split by the fluorine atom through three bonds, with coupling constant $^{3}J_{H-F}$ = 13.38 Hz. The H3 proton appears as doublet at 7.2936 and 7.2816 ppm split by the fluorine atom through four bonds, with coupling constant $^{4}J_{H-F}$ = 7.22 Hz. Protons at position 11 (H11) appear as quartet at 4.65, 4.64, 4.627 and 4.615 ppm due to three bond coupling with three H12 protons. H15 and H19 appear at 3.9 ppm and 3.58 ppm. H16, H18 appear at 3.27 and 2.9 ppm. Signal for protons at position 20 (H20) appear as a singlet at 2.32 ppm. H12 protons split into triplet at 1.44, 1.429 and 1.417 ppm due to three bond coupling with H11 protons. As shown in ^{13}C NMR Spectra C1 peak split into doublet with one bond coupling constant $^{1}J_{C-F}$= 253 Hz. C6 also appears as a doublet through two bonds with coupling constants $^{2}J_{C-F}$= 21.66 Hz.

^{13}C	Chemical shift	^{13}C	Chemical shift
C12	13.59	C6	110.28,110.14
C20	38.53	C5	136.32
C11	42.47	C4	143.94
C15	46.29	C2	146.74
C18	49.92	C1	151.46
C16, C18	52.87	C8	153.14
C3	104.96	C21	167.71
C9	118.01	C10	174.2

Table 3.4: ^{13}C chemical shift values (in ppm) for Pefloxacin

3.3 2D experiments

The standard pulse program cosyph, cosygpqf, hsqcetgp, hmbcgplpndqf, hmqcgpqf, hfcoqfqn were used to record 2D ^{1}H-^{1}H COSY, ^{1}H-^{13}C HSQC, ^{1}H-^{13}C HMBC, ^{1}H-^{19}F HOESY NMR spectra for these drugs. 2D spectra hmqcgpqf were acquired using QF Fnmode, hsqcetgp were acquired using Echo-Antiecho method and others are acquired using States-TPPI method with 2048 FID in t_2 and 256 FID in t_1 dimension.

Following figure shows the 2D homonuclear ^{1}H-^{1}H COSY for Flumequine. Their chemical shifts are assigned in 1D spectra of ^{1}H, 13C and ^{19}F spectra. Homonuclear ^{1}H-^{1}H COSY shows cross peak for H8-H15 and H9-H10 which are coupled to each other.

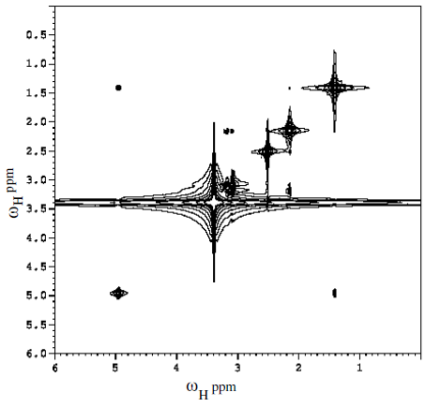

Figure 3.15: 2D ^{1}H-^{1}H COSY spectra of Flumequine in DMSO solvent.

2D homonuclear ^{1}H-^{1}H COSY, 2D heteronuclear ^{1}H-^{13}C HMBC, ^{1}H-^{13}C HSQC for Levofloxacin are shown in the following figure. Their chemical shifts are assigned in 1D spectra of ^{1}H, 13C and ^{19}F spectra. Homonuclear ^{1}H-^{1}H COSY shows cross peak for H19-H20 at (1.45 ppm, 4.92 ppm) and (4.92 ppm, 1.45 ppm). Another cross peak appear for H15-H15 (two different proton at position 15) and H23,H25- H22,H26 in the spectra.

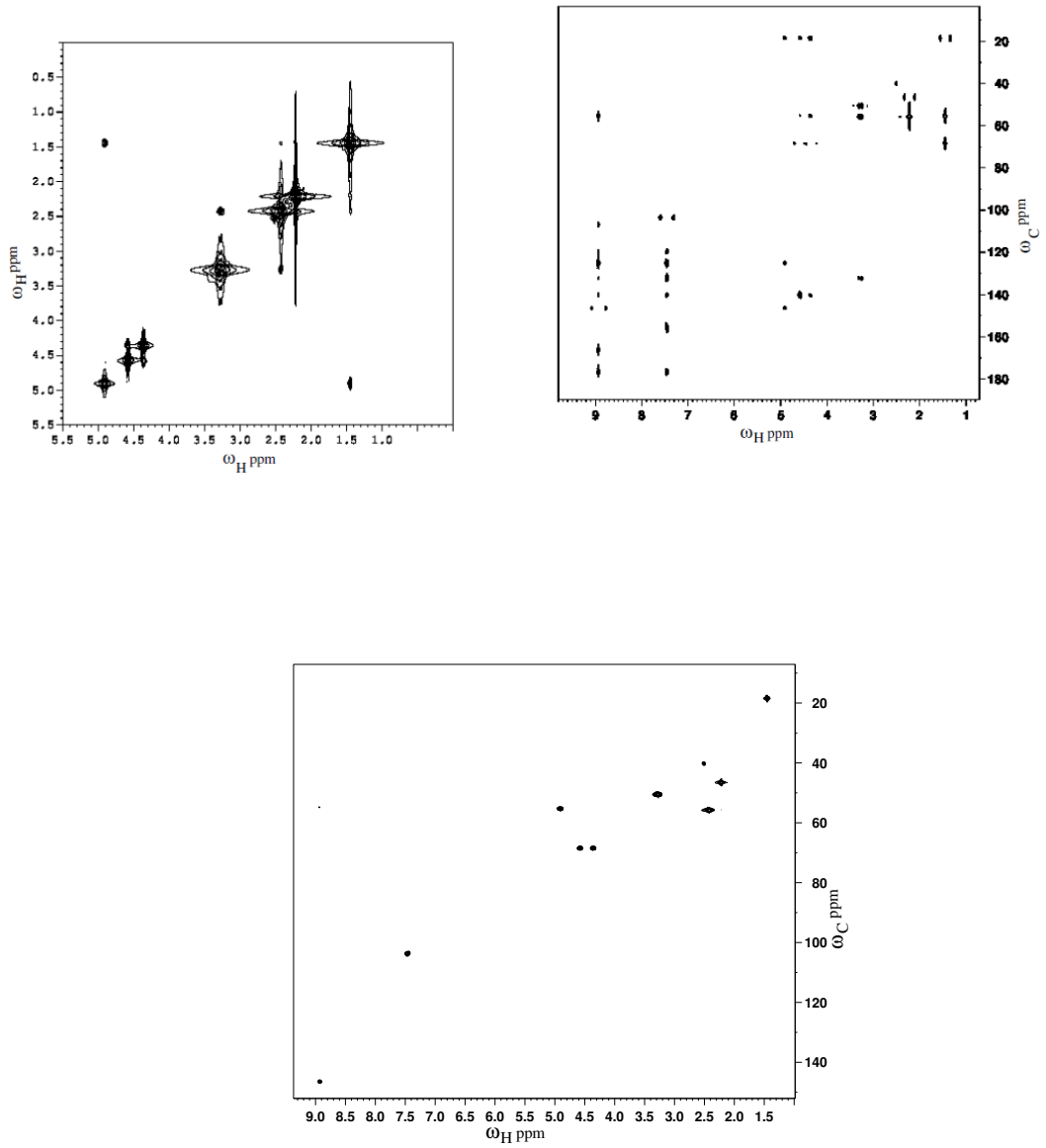

Figure 3.16: 2D ^{1}H-^{1}H COSY, ^{1}H-^{13}C HMBC and ^{1}H-^{13}C HSQC spectra of Levofloxacin in DMSO solvent.

2D homonuclear ^{1}H-^{1}H COSY, 2D heteronuclear ^{1}H-^{13}C HMQC, ^{1}H-^{13}C HSQC for Pefloxacin are shown in the following figure. Their chemical shifts are assigned in 1D spectra of ^{1}H, 13C and ^{19}F spectra. Homonuclear ^{1}H-^{1}H COSY show cross peaks for H11-H12 and H16,H18-H20 due to their coupling. Each peak in the ^{1}H-^{13}C HSQC spectrum represents a bonded C-H pair, with its two coordinates corresponding to the chemical shifts of each of the H and C atoms.[29]

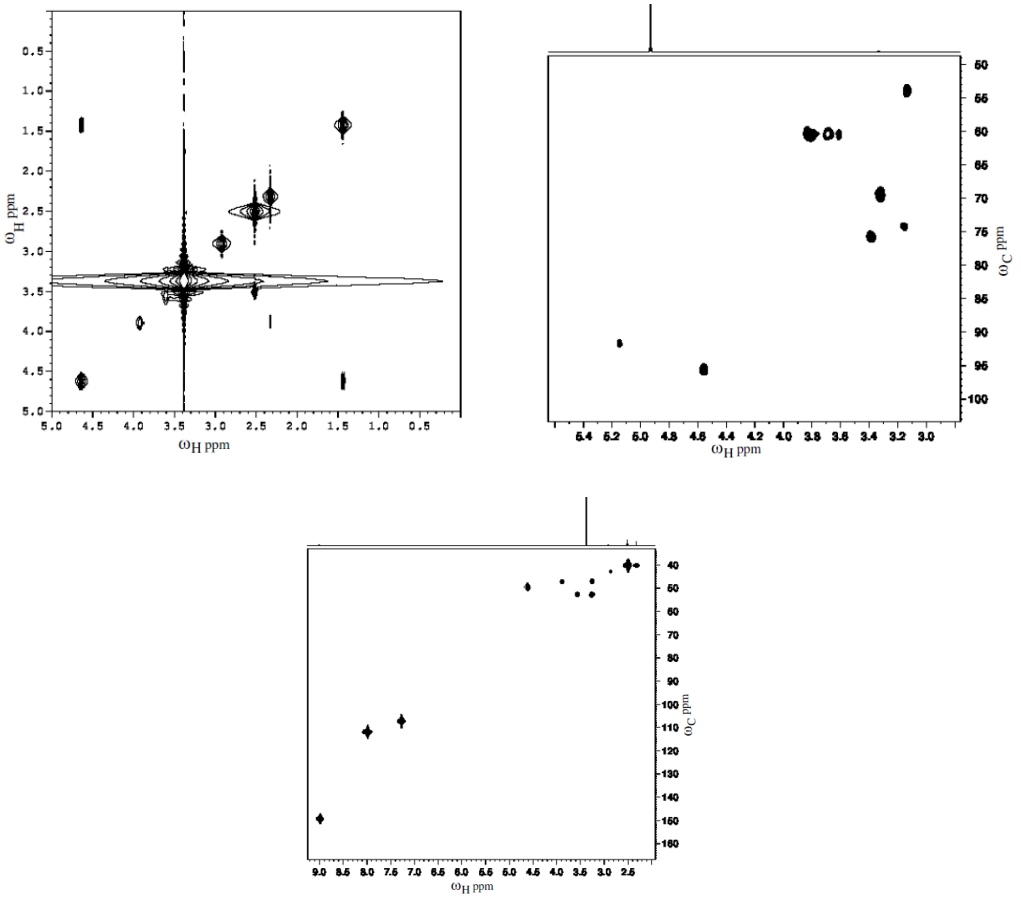

Figure 3.17: 2D ^{1}H-^{1}H COSY, ^{1}H-^{13}C HMQC and ^{1}H-^{13}C HSQC spectra of Pefloxacin in D_2O solvent.

2D heteronuclear ^{1}H-^{13}C HMQC, ^{1}H-^{13}C HSQC and hetcor ^{1}H-^{19}F for Difloxacin are shown in the following figure. Their chemical shifts are assigned in 1D spectra of ^{1}H, 13C and ^{19}F spectra. Each peak in the ^{1}H-^{13}C HSQC spectrum represents a bonded C-H pair, with its two coordinates corresponding to the chemical shifts of each of the H and C atoms.[29] Hetcor spectrum of ^{1}H-^{19}F shows cross peaks at (7.6 ppm,

-110.27 ppm) due to F(18) and their coupled protons, cross peaks were observed at (8.1 ppm, -121.5 ppm) and (6.5 ppm, -121.5 ppm) due to F(17) and coupled proton.

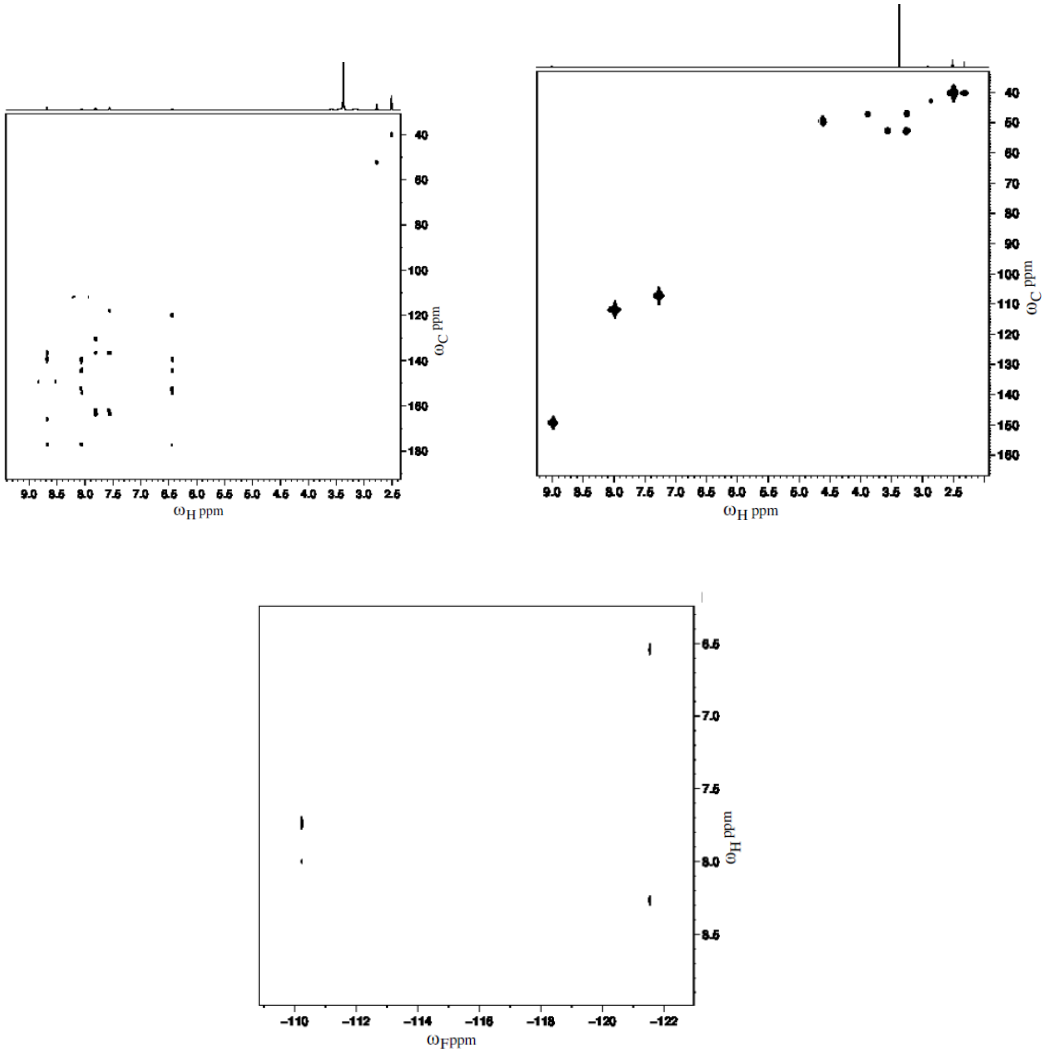

Figure 3.18: 2D ^{1}H-^{1}H COSY, ^{1}H-^{13}C HMQC and ^{1}H-^{13}C HSQC spectra of Difloxacin in DMSO solvent.

3.4 Diffusion Measurement

1D ^{1}H and ^{19}F diffusion experiments of these fluoroquinolones were done using Bruker standard pulse sequence *ledbpgp2s1d*. Diffusion ^{1}H NMR spectra of fluoroquinolnes were obtained with 20 ppm spectral width using experimental parameters: number of

scan = 16, processed with SI = 64k, TD = 132k, D1 = 1 s and line broadening (LB) = 0.3Hz. Sine shaped gradients were applied which cover the range of 5% to 95 % of the maximum gradient strength. Experiments were done with a single-axis actively shielded Z-gradient capable of achieving a maximum gradient strength of 53.5 Gcm^{-1}. NMR data processing was done using Bruker Topspin 2.1 software.

Molecule	Nuclei	D (m^2/s)	Nuclei	D (m^2/s)
Flumequine	H(1)	2.95 $\times 10^{-10}$	F(19)	2.98 $\times 10^{-10}$
	H(5)	2.27 $\times 10^{-10}$		
Levofloxacin	H(3)	2.36 $\times 10^{-10}$	F(12)	2.98 $\times 10^{-10}$
Pefloxacin	H(6)	2.03 $\times 10^{-10}$	F(13)	2.61 $\times 10^{-10}$
	H(3)	3.26 $\times 10^{-10}$		
Fleroxacin	H(27)	2.44 $\times 10^{-10}$	F(12)	2.77 $\times 10^{-10}$
Difloxacin	H(6)	2.01 $\times 10^{-10}$	F(18)	2.72 $\times 10^{-10}$
	H(3)	1.99 $\times 10^{-10}$	F(17)	9.4 $\times 10^{-11}$

Table 3.5: Diffusion coefficients calculated using GNUPLOT software from 1D ^{1}H and ^{19}F diffusion experiments.

3.5 Measurement of Relaxation times

Experimental time constants the these five fluorinated system were calculated using t1ir1d and cpmg1d experiments. We have calculated relaxation time for ^{1}H, ^{13}C and ^{19}F, which are coupled to each other on the aromatic ring in molecule structure.

molecule	nuclei	T_1	T_2	nuclei	T_1	T_2
Flumequnie	H(1)	2.61 s	2.5 s	F(19)	0.5829 s	0.44 s
	H(5)	1.75 s	1.46 s			
Levofloxacin	H(3)	2.23 s	2.21 s	F(12)	0.3058 s	0.20 s
Pefloxacin	H(6)	2.22 s	1.89 s	F(3)	0.445 s	0.36 s
	H(3)	0.45 s	0.36 s			
Fleroxacin	H(27)	2.18 s	1.92 s	F(12)	0.34 s	0.13 s
				F(28)	0.47 s	0.29 s
Difloxacin	H(6)	2.19 s	0.58 s	F(18)	0.23 s	0.1 s
	H(3)	0.81 s	0.38 s	F(17)	0.43	0.25 s

Table 3.6: T_1 and T_2 for ^{1}H and ^{19}F time constant of all five fluoroquinolones

molecule	nuclei	T_1	nuclei	T_1	nuclei	T_1
Prulifloxacin	C1	0.354 s	C2	0.350 s	C6	0.157 s
Flumequine	C6	0.366 s	C5	0.37 s	C1	0.186 s
Levofloxacin	C4	0.74 s	C5	0.453 s	C3	0.167 s
Pefloxacin	C1	0.403 s	C2		C6	0.156 s
Difloxacin	C1		C2	0.556 s	C6	0.18 s

Table 3.7: T_1 time constant of ^{13}C spins.

3.6 Conclusion

1-D and 2-D NMR experiments were performed and relaxation times were calculated for all the fluorinated drugs for nuclei ^{1}H, ^{13}C and ^{19}F. ^{13}C relaxation time can be used to calculate the correlation time of the ^{13}C nuclei. Diffusion coefficient for ^{1}H and ^{19}F nuclei were calculated for all the five drugs.

Chapter 4

Characterization of ^{19}F CSA tensor of fluoroquinoles

4.1 CSA tensor

When an external magnetic field is applied then the electrons orbiting around the nucleus induce a local magnetic field. This magnetic field then leads to chemical shift. The spatial geometry of the system and electronic structure is responsible for these fields. This chemical shift can be described using a chemical shift tensor.[30,31] Tensor is an important tool to study the internal dynamics at atomic resolutions. It can be used to interpret the NMR relaxation data which then give us information about the molecular dynamics of a system.[32,33,34] Brownian Motion in a liquid limits the value of chemical shift tensor to one third of its trace which is known as isotropic chemical shift. Thus it becomes a challenging job to determine the chemical shielding tensor accurately. Quantum chemical calculations provide great help in these type of cases where there is a lack in information.[35,36]

If the overall motion of a system of molecules can be defined using an axially symmetric diffusion tensor, then using a generalized model independent approach for these system of molecules, we can calculate the chemical shift anisotropic (CSA) tensor parameter using the longitudinal and transverse auto and cross correlated relaxation rates.[37] The cross correlated spin relaxation rate provide valuable information about what is going on in system in case of liquid NMR. Thus, it provides important details about the molecular structure and the dynamics. Relaxation study of fluorinated drugs helps to investigate their binding affinity, their binding site and bioavailability.

^{19}F CSA tensor is an essential tool in NMR to investigation biomolecules. The polarization and coherence transfer leads to correlated fluctuations of different interactions which then leads to the cross correlated relaxation phenomenon.[38] Various experiments have been developed to study the cross correlated relaxations and to determine the cross correlated relaxation rates.[39]

From the study that has been done for several decades, it is evident that the longitudinal Chemical shift anisotropy and dipolar relaxation.[40] The longitudinal CSA-dipolar cross correlation is quite difficult to measure.[38] Recent methods involving gradient based sequences have been proposed to determine longitudinal CSA-dipolar cross correlation rates.[41] CSA-DD cross correlated rates have been used to determine the NMR chemical shielding tensor (σ) elements and also their relative orientations in the molecular frame. Theoretical analysis of NMR parameters tells us information about how these parameters are dependent on molecular structure. Thus theoretical modelling using quantum chemistry is used as an essential tool while doing NMR experiments.[42]

CSA tensor of NMR active nuclei are determined using quantum chemical methods when it is hard to get using spectroscopic methods. CSA tensor are important in determining structure and dynamics. The magnitude and orientation of the CSA tensor for a few NMR active nuclei have been determined using quantum chemical calculations. Results of the quantum chemical calculations and experimentally determined values were reasonably matched.

This chapter focuses on determining CSA tensor of ^{19}F using quantum chemical calculations and experimental study of some non-equivalent fluorinated systems. Liquid state NMR pulse sequences can be used to measure cross correlated spin relaxation between the CSA of fluorine and its dipolar interaction with other spins like proton. In ^{19}F NMR, chemical shift dispersion is much larger than ^{1}H NMR and due to its higher gyromagnetic ratio and high abundance it is widely useful. Its high sensitivity to change in the local environment is the unique property which makes it useful to study biological systems. ^{19}F CSA tensor has large anisotropy values and it is used as a useful structural marker. Quantum chemical calculations of CSA tensor are done using Gaussian09 software. Chemical shift depends on the local electronic structure and orientation of molecular orbitals and it can be described using a chemical shift tensor. Three principal values of the tensor provide the information necessary to describe the

CSA of a nuclear spin. The chemical shift anisotropy tensor can be mathematically represented as a tensor of rank 2. For isotropically tumbling molecules in solution, the CSA is averaged out to give an isotropic chemical shift. The CSA tensor characterizes the magnitude and the orientation dependence of the chemical shift and is represented by a 3 × 3 matrix.

4.2 Inversion recovery experiment of ^{19}F

The experimental spectra corresponding to various two-spin order modes are shown for the set of fluoroquinolones in the following figures. Unequal relaxation of different ^{19}F lines of the fluorine spin multiplet is clear evidence for the presence of CSA-DD cross-correlations.

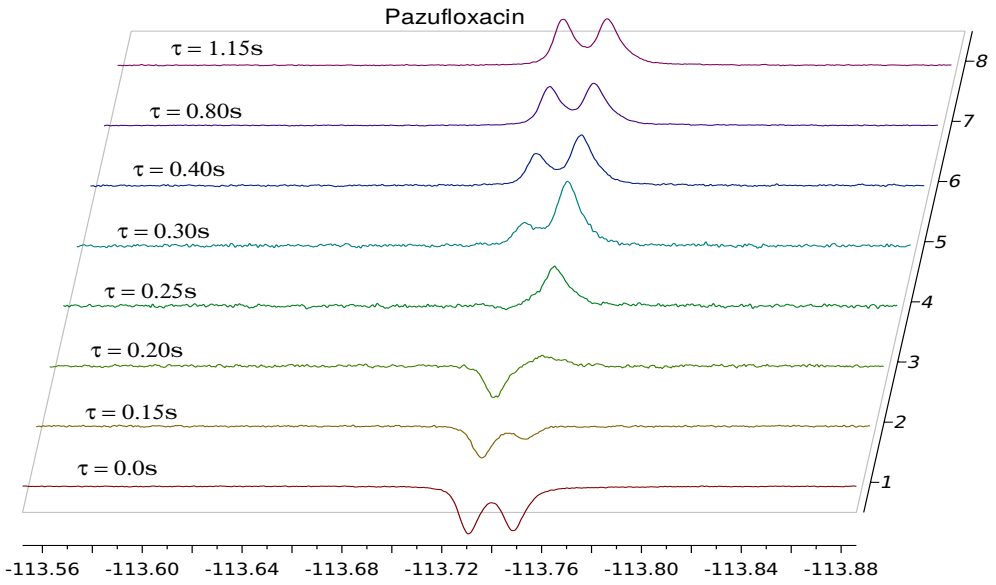

Figure 4.1: The ^{19}F spectra of pazufloxacin for different recovery times obtained from the inversion recovery experiment. The differential relaxation of the fluorine multiplet shows the emergence and buildup of longitudinal two-spin order for this weakly coupled AX spin system.

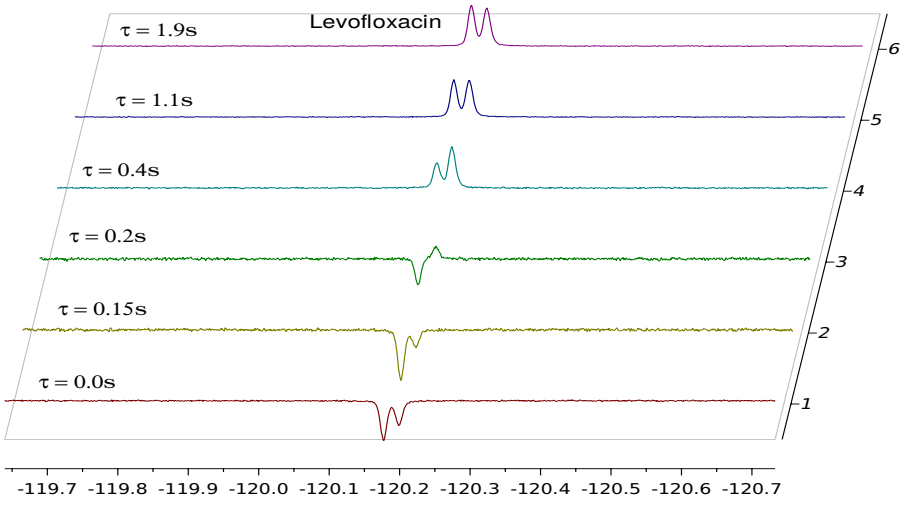

Figure 4.2: The ^{19}F spectra of levofloxacin for different recovery times obtained from the inversion recovery experiment. The differential relaxation of the fluorine multiplet shows the emergence and buildup of longitudinal two-spin order for this weakly coupled AX spin system.

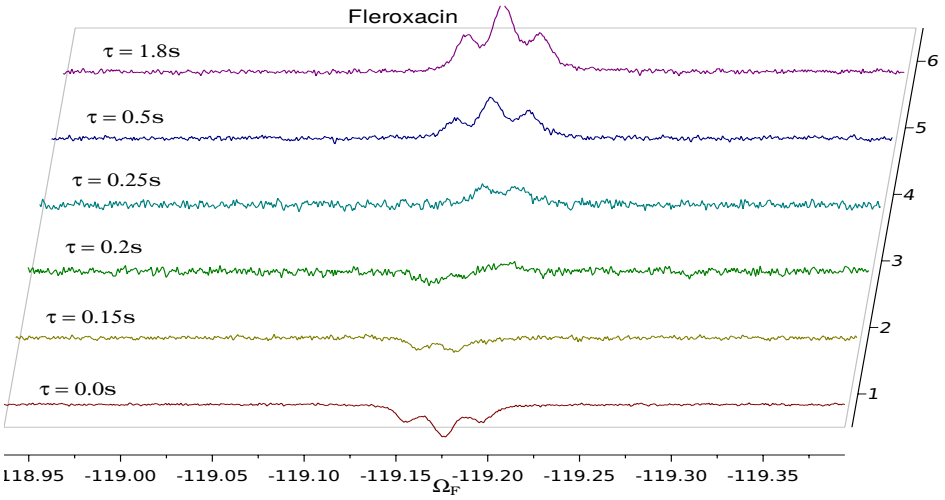

Figure 4.3: The ^{19}F spectra of fleroxacin for different recovery times obtained from the inversion recovery experiment. The differential relaxation of the fluorine multiplet shows the emergence and buildup of longitudinal two-spin order for this weakly coupled A_2X spin system.

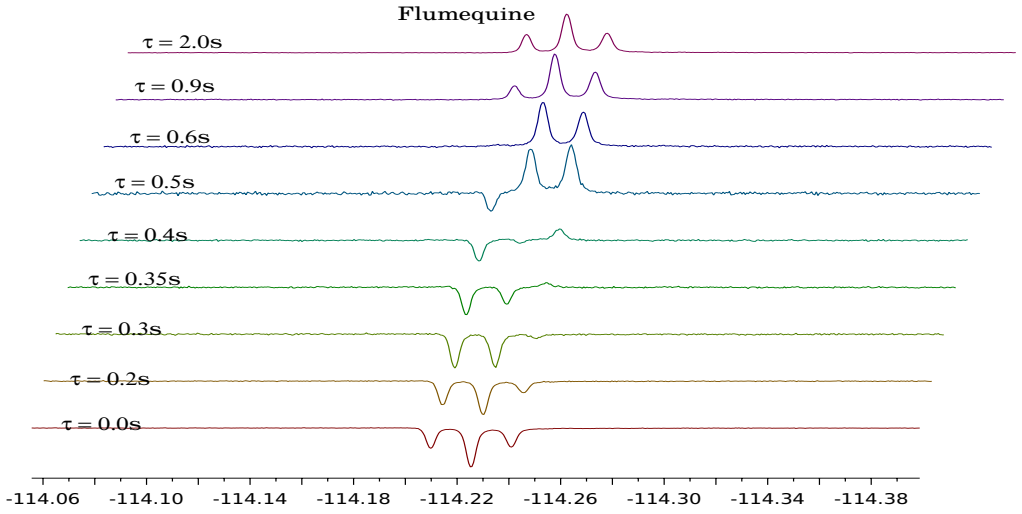

Figure 4.4: The ^{19}F spectra of flumequine for different recovery times obtained from the inversion recovery experiment. The differential relaxation of the fluorine multiplet shows the emergence and buildup of longitudinal two-spin order for this weakly coupled AX_2 spin system.

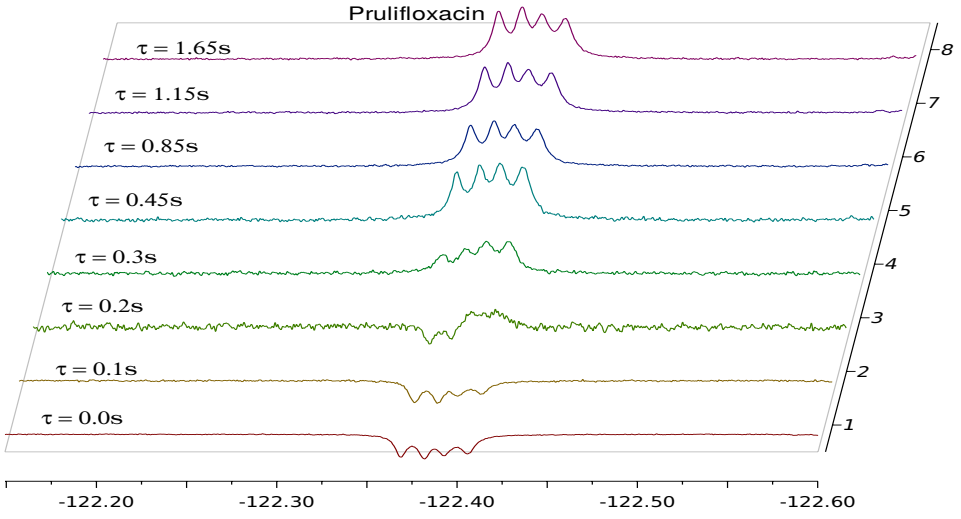

Figure 4.5: The ^{19}F spectra of prulifloxacin for different recovery times obtained from the inversion recovery experiment. The differential relaxation of the fluorine multiplet shows the emergence and buildup of longitudinal two-spin order for this weakly coupled AMX spin system.

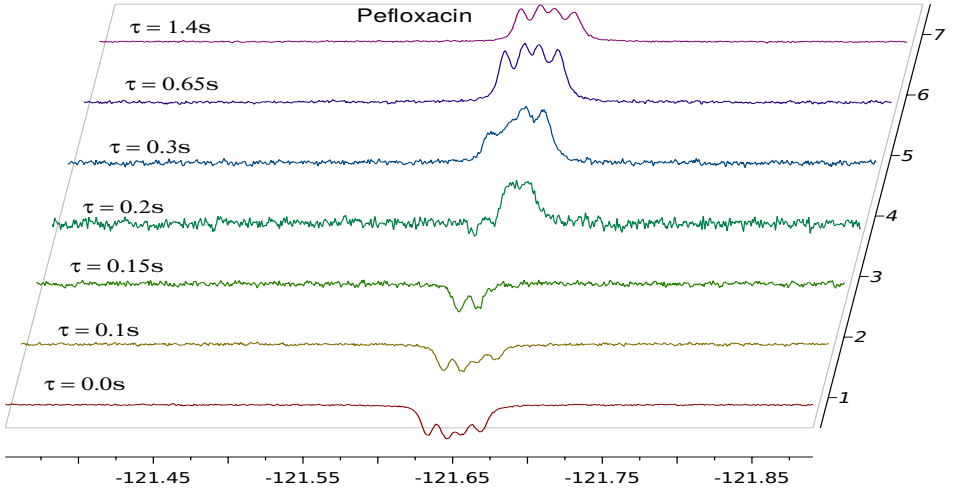

Figure 4.6: The ^{19}F spectra of pefloxacin for different recovery times obtained from the inversion recovery experiment. The differential relaxation of the fluorine multiplet shows the emergence and buildup of longitudinal two-spin order for this weakly coupled AMX spin system.

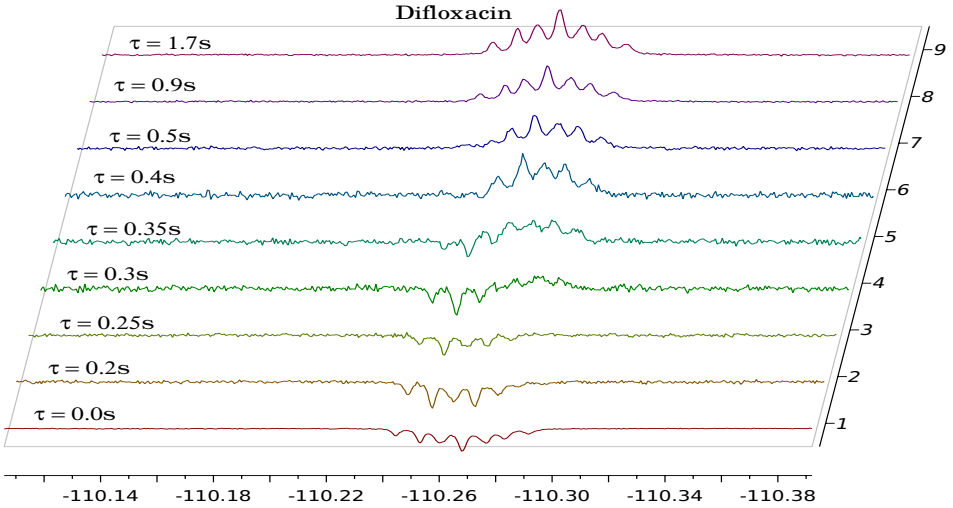

Figure 4.7: The ^{19}F spectra of difloxacin for different recovery times obtained from the inversion recovery experiment. The differential relaxation of the fluorine multiplet shows the emergence and buildup of longitudinal two-spin order for this weakly coupled AM_2X_2 spin system.

4.3 Quantum Chemical Calculations

^{19}F CSA tensor were determined using quantum chemistry calculations. The structure of the fluorinated drugs were built using Gaussview 4.1 package and then geometry optimization was done using Gaussian09 program. Gaussian is a computational chemistry program capable of predicting many properties of the molecules and reactions such as molecular energy, structure and NMR properties. Geometry optimization was done using HF/6-31g basis set using the Hartree-Fock method and after geometry optimization, the ^{19}F CSA tensor calculation was done with gauge including atomic orbitals (GIAO) combined with HF and DFT methods using a large basis set [Dit74, WHP90, HAB+92]. CSA tensor calculations were performed using HF/sto-3g, HF/sto-3g*, HF/sto-3g**, HF/3-21g, HF/6-31g, HF/6-311g, b3lyp/3-21g, b3lyp/6-31g, b3lyp/6-311g basis sets. All quantum chemistry calculations were performed using the Gaussian09 software package. For ^{19}F $CFCl_3$ was used as a reference compound.

The simplest *ab initio* method in which correlated electron-electron repulsion is not specifically taken into account in the HF method. Only the average of the correlated electron-electron repulsion is taken into calculation. It provides first level predictions for systems at an initial stage. While HF method is popular, in last few years, method based on density functional theory has become more popular as it gives better accuracy at a manageable computational cost. There are methods which improve upon the HF method. Moeller-Plesset perturbation theory (MP) is one such post-Hartree-Fock *ab initio* method which adds electron correlation effect by means of Rayleigh-Schroedinger perturbation theory (RS-PT) to the higher orders, second to fourth (MP2, MP3, MP4) usually. But this method is rarely used due to the high computational costs involved.

The level of detail of the calculations dictates the effects of electron correlation on the calculation of chemical shielding tensors as has been shown.[43, 44, 45] In the MP2-GIAO methods, isotropic shifts and in-plane components of the shielding are underestimated and the tensor element perpendicular to the ring plane is overestimated.[46] For the particular case of fluorine, DFT should not be used as the inclusion of electron correlation in general results in the chemical shielding tensor elements being overestimated. Additionally, larger number of surrounding electrons lead to larger estimation of shielding constant.[43, 45] HF methods outperform MP or DFT calculations in systems such as

amino acids or fluoroaromatics where electron correlation is unimportant.[43] Though dynamic electron-correlation needs to be included for accurate geometry optimization, it as been previously noted that the MP2-GIAO and DFT-GIAO methods result in overestimation of the experimental ^{19}F chemical shifts when compared with HF method.[46]

CSA tensor is completely characterized by its principal elements and from these ^{19}F CSA tensor values, CSA parameters span (Ω), skew (κ) and isotropic chemical shift σ_{iso}, δ_{iso} for ^{19}F were determined.

$$\begin{aligned}
\Omega &= \sigma_{33} - \sigma_{11}, \qquad (\Omega > 0) \\
\kappa &= (2\sigma_{22} - \sigma_{11} - \sigma_{33})/\Omega, \qquad (-1 \leq \kappa \leq 1) \\
\sigma_{iso} &= \frac{1}{3}(\sigma_{11} + \sigma_{22} + \sigma_{33}) \\
\delta_{ii} &= \sigma_{ii,ref} - \sigma_{ii}, \qquad i = 1, 2, 3 \\
\delta_{iso} &= \frac{1}{3}(\delta_{11} + \delta_{22} + \delta_{33})
\end{aligned} \tag{4.1}$$

where the principal component of the CSA tensors follow the Herzfeld-Berger convention $\sigma_{11} \leq \sigma_{22} \leq \sigma_{33}$ and $\sigma_{ii,ref}$ refers to the principal component of the CSA tensor of the reference compound used, $CFCl_3$ is the reference compound here. In the tables all principal components are estimated in terms of σ_{xx}, σ_{22},σ_{33} instead of σ_{11}, σ_{22}, σ_{33} similarly they follow convention $\sigma_{xx} \leq \sigma_{yy} \leq \sigma_{zz}$. The CSA of ^{19}F spin can be estimated from liquid state relaxation experiments by measuring the cross-correlated relaxation between the CSA of a specific spin (^{19}F) and its dipolar interaction with other spins like proton. We are interested in accurately measuring the CSA-DD cross correlation rates between the ^{19}F CSA and ^{19}F-^{1}H dipolar interaction. The CSA/DD relaxation rate constant is given by[47]

$$\Delta^F_{HF} = \frac{2}{5}\,\frac{\mu_0}{4\pi}\,\frac{\gamma_F^2\gamma_H\hbar B_0}{r^3_{HF}}\frac{\tau_c}{1+\omega_F^2\tau_c^2}(\Delta\sigma_g)^F$$

where τ_c is the overall correlation time and $\Delta\sigma_g^F$ is a "geometric" CSA parametergiven for an axially symmetric CSA tesor by

$$\Delta\sigma_g^F = \Delta\sigma_F[\frac{1}{2}(3\cos^2\theta_{F,FX} - 1)] \tag{4.2}$$

where $\theta_{F,FX}$ is the angle subtended by the internuclear FX vector and the symmetric axis of the CSA tensor. $\Delta\sigma_g^F$ contains both magnitude and orientation information it has been termed as a "geometric" CSA parameter. In general for most molecules it has been observed that the fluorine CSA tensor is not axially symmetric and hence can be written as a sum of two axially symmetric tensors with their symmetry axes oriented along two orthogonal directions (x,y).[48] The geometric CSA parameter $\Delta\sigma_g^F$ then becomes

$$\Delta\sigma_g^F = (\Delta\sigma_x)^F[\frac{1}{2}(3\cos^2\phi_x - 1)] + (\Delta\sigma_y)^F[\frac{1}{2}(3\cos^2\phi_x - 1)] \tag{4.3}$$

where $\Delta\sigma_i$, $i = x, y$ is the anisotropy of the axially symmetric shielding tensor with its symmetric axis along i and the angle ϕ_i refers to the orientation of the FX bond vector with respect to the symmetry axis of the CSA tensor oriented along the i axis. Tables 4.1- 4.9 show the results of the CSA tensor computation in terms of the tensor principal elements computed using HF and DFT methods with large basis sets.

Table 4.1: Principal axis component (σ in ppm) of ^{19}F CSA tensor for $CFCl_3$ computed using HF and DFT methods with different basis sets.

Method	σ_{xx}	σ_{yy}	σ_{zz}	σ_{iso}	σ_{aniso}	Ω	κ
hf/sto-3g	356.3856	375.1292	375.1554	368.8901	9.3980	18.77	0.997
hf/3-21g	246.5735	246.5944	292.0905	261.7528	45.5065	45.52	-0.99
hf/6-31g	195.6474	195.6672	293.3413	228.2186	97.6841	97.69	-0.99
hf/6-311g	173.6396	173.6593	277.5991	208.2993	103.9496	103.96	-0.99
b3lyp/3-21g	155.6481	155.6860	160.5107	157.2816	4.8436	4.86	-0.984
b3lyp/6-31g	113.4492	113.4916	179.3617	135.4342	65.8913	65.91	-0.998
b3lyp/6-311g	89.6275	89.6677	156.7332	112.0095	67.0856	67.01	-0.998

Table 4.2: Principal axis component (δ in ppm) of ^{19}F CSA tensor for for flumequine computed using HF and DFT methods with different basis sets.

Method	δ_{xx}	δ_{yy}	δ_{zz}	δ_{iso}
hf/sto-3g	59.136	-1.811	-111.865	-18.180
hf/3-21g	-56.687	-140.816	-135.929	-111.144
hf/6-31g	-77.603	-185.793	-97.719	-120.372
hf/6-311g	-98.921	-207.511	-107.731	-138.054
b3lyp/3-21g	-58.202	-159.024	-227.78	-148.335
b3lyp/6-31g	-79.511	-205.998	-172.618	-152.709
b3lyp/6-311g	-97.413	-234.082	-182.507	-171.334

Table 4.3: Principal axis component (δ in ppm) of ^{19}F CSA tensor for for levofloxacin computed using HF and DFT methods with different basis sets.

Method	δ_{xx}	δ_{yy}	δ_{zz}	δ_{iso}
hf/sto-3g	46.016	-1.691	-116.055	-23.91
hf/3-21g	-86.8965	-142.286	-153.529	-127.571
hf/6-31g	-109.323	-176.783	-116.729	-134.278
hf/6-311g	-131.98	-200.90	-123.281	-152.054
b3lyp/3-21g	-97.042	-166.584	-251.169	-171.598
b3lyp/6-31g	-117.081	-199.638	-196.258	-170.993
b3lyp/6-311g	-137.363	-225.212	-207.907	-190.161

Table 4.4: Principal axis component (δ in ppm) of ^{19}F CSA tensor for for pefloxacin computed using HF and DFT methods with different basis sets.

Method	δ_{xx}	δ_{yy}	δ_{zz}	δ_{iso}
hf/sto-3g	39.626	-5.351	-119.3045	-28.343
hf/3-21g	-90.426	-141.886	-159.389	-130.567
hf/6-31g	-112.643	-173.363	-126.599	-137.535
hf/6-311g	-135.020	-198.031	-138.391	-157.147
b3lyp/3-21g	-93.492	-161.284	-261.889	-172.222
b3lyp/6-31g	-113.111	-191.308	-210.708	-171.709
b3lyp/6-311g	-132.7125	-218.123	-228.907	-193.247

Table 4.5: Principal axis component (δ in ppm) of ^{19}F CSA tensor for for fleroxacin computed using HF and DFT methods with different basis sets.

Method	δ_{xx}	δ_{yy}	δ_{zz}	δ_{iso}
hf/sto-3g	43.956	-2.501	-115.815	-24.786
hf/3-21g	-88.286	-143.426	-150.499	-127.404
hf/6-31g	-111.17	-175.913	-113.789	-133.625
hf/6-311g	-134.22	-200.021	-122.031	-152.091
b3lyp/3-21g	-94.772	-166.204	-247.289	-169.422
b3lyp/6-31g	-114.881	-196.708	-192.768	-168.120
b3lyp/6-311g	-134.6825	-222.092	-206.237	-187.671

Table 4.6: Principal axis component (δ in ppm) of ^{19}F CSA tensor for for fleroxacin computed using HF and DFT methods with different basis sets.

Method	δ_{xx}	δ_{yy}	δ_{zz}	δ_{iso}
hf/sto-3g	-96.654	-79.280	-97.875	-91.269
hf/3-21g	-196.6365	-216.086	-219.759	-210.827
hf/6-31g	-240.6326	-241.933	-196.888	-226.485
hf/6-311g	-256.690	-262.911	-211.311	-243.637
b3lyp/3-21g	-248.832	-263.034	-306.089	-272.652
b3lyp/6-31g	-274.771	-289.018	-269.798	-277.863
b3lyp/6-311g	-292.793	-313.502	-294.057	-300.117

Table 4.7: Principal axis component (δ in ppm) of ^{19}F CSA tensor for for fleroxacin computed using HF and DFT methods with different basis sets.

Method	δ_{xx}	δ_{yy}	δ_{zz}	δ_{iso}
hf/sto-3g	21.006	-10.521	-127.685	-39.067
hf/3-21g	-142.136	-149.166	-175.159	-155.487
hf/6-31g	-161.563	-167.563	-143.468	-157.532
hf/6-311g	-185.701	-187.801	-154.701	-176.067
b3lyp/3-21g	-155.132	-182.704	-278.229	-205.355
b3lyp/6-31g	-169.571	-195.198	-228.558	-197.776
b3lyp/6-311g	-193.223	-214.812	-245.577	-217.870

Table 4.8: Principal axis component (δ in ppm) of ^{19}F CSA tensor for for difloxacin computed using HF and DFT methods with different basis sets.

Method	δ_{xx}	δ_{yy}	δ_{zz}	δ_{iso}
hf/sto-3g	17.256	-8.971	-129.535	-40.417
hf/3-21g	-114.786	-146.176	-165.9895	-142.317
hf/6-31g	-137.963	-176.763	-131.038	-148.588
hf/6-311g	-160.42	-200.721	-138.131	-166.424
b3lyp/3-21g	-120.582	-171.234	-267.609	-186.475
b3lyp/6-31g	-139.861	-199.598	-214.368	-184.609
b3lyp/6-311g	-159.9525	-224.522	-227.147	-203.874

Table 4.9: Principal axis component (δ in ppm) of ^{19}F CSA tensor for for difloxacin computed using HF and DFT methods with different basis sets.

Method	δ_{xx}	δ_{yy}	δ_{zz}	δ_{iso}
hf/sto-3g	59.596	13.789	-128.775	-18.463
hf/3-21g	-40.736	-120.416	-149.049	-103.401
hf/6-31g	-63.223	-167.723	-111.478	-114.141
hf/6-311g	-83.430	-191.931	-117.691	-131.017
b3lyp/3-21g	-54.682	-137.574	-242.779	-145.011
b3lyp/6-31g	-77.99	-187.398	-188.308	-151.23
b3lyp/6-311g	-94.302	-212.652	-198.327	-168.427

4.4 Conclusion

^{19}F CSA tensor is used to characterize biomolecules structure and their orientations. Quantum chemistry calculations were performed using HF and DFT theory with a large basis set to compute the ^{19}F CSA tensor. It was found that computationally calculated ^{19}F CSA tensor using HF method with 3-21g basis set matches well with the experimental observed chemical shift values. Particularly in the case of fluorine due to presence of large number of electrons, DFT and MP2 theory overestimate the CSA tensor values. Thus, in systems where electron correlation is unimportant, HF

method perform better than DFT and MP2 methods. Relaxation experiments were done to characterize the ^{19}F CSA tensor of fluorinated drugs experimentally. We hope that ^{19}F NMR strategy will be helpful in future studies to explore the role of the fluorine CSA tensor as structure predictor and in understanding the dynamics of fluorinated biomolecules.

Bibliography

[1] Keeler, J. *Understanding NMR Spectroscopy*; Wiley, 2002.

[2] Freeman., R. *Spin choreography.*; Spektrum Academic Publishers: Oxford, U.K., 1997.

[3] Uhlenbeck, G. E.; Goudsmit., S. A. *Naturwis-senschaften* **1925**, *47*, 953–954.

[4] Cavanagh, J.; Fairbrother, W. J.; Palmer, A. G.; Rance, M.; Skelton., N. J. *Protein NMR spectroscopy.*, 2nd ed.; Elsevier Academic Press,: London, U.K., 2007.

[5] McNaught, A. D.; Wilkinson., A. *IUPAC compendium of chemical terminology (the Gold book)*, 2nd ed.; Blackwell Scienti
c Publications: Oxford, U.K., 1997.

[6] Levitt, M. H. *Spin dynamics*; John Wiley & Sons Ltd.: Chichester, U.K., 2008.

[7] Zimmerman, J. R.; Williams., D. *Phys. Rev.* **1949**, *76*, 350–357.

[8] Veeman, W. S. *Prog. Nuc. Magn. Reson.* **1984**, *16*, 193–235.

[9] Waugh, J. S.; Haeberlen, U. *Academic Press* **1976**,

[10] Robyr, P.; Meier, B. H.; Ernst, R. R. *Chem. Phys. Lett.* **1991**, *187*, 471–478.

[11] Robyr, P.; Meier, B. H.; Ernst, R. R. *J. Am. Chem. Soc.* **1994**, *116*, 5315–5323.

[12] Henrichs, P. M.; Linder, M. *J. Magn. Reson.* **1984**, *58*, 458–461.

[13] Tossell, J. A. *Nuclear Magnetic Shieldings and Molecular structure. NATO ASI series: Mathematical and Physical properties.*; Kluwer Academic Publishers, 1993.

[14] Lipkowitz, K. B.; Boyd, D. B. *Reviews in Computational Chemistry*; John Wiley & Sons, 1996.

[15] Levine, I. N. *Quantum Chemistry*, 6th ed.; PHI Learning Ltd.: New Delhi, 2010.

[16] Szabo, A.; Ostlund, N. S. *Modern Quantum Chemistry*; Dover Publications, Inc.:Mineola: New York, 1996.

[17] F.Morris, K.; Johnson, C. S. *J. Am. Chem. Soc.* **1992**, *114*, 3139.

[18] Bloch., F. *Phys. Rev.* **1946**, *70(7-8)*, 460–474.

[19] Bloch, F.; Hansen, W. W.; Packard., M. E. *Phys. Rev.* **1946**, *70(7-8)*, 474–485.

[20] Ernst, R. R.; Bodenhausen, G.; Wokaun, A. *Principles of nuclear magnetic resonance in one and two dimensions.*; Oxford University Press: Oxford, U.K., 1988.

[21] Hahn, E. L. *phys. rev.* **1949**, *76(1)*, 145–146.

[22] Vold, R. L.; Waugh, J. S.; Klein, M. P.; Phelps., D. E. *J. Chem. Phys.* **1968**, *48(8)*, 3831–3832.

[23] Hahn., E. L. *Phys. Rev.* **1950**, *77(2)*, 297–298.

[24] Hahn., E. L. *Phys. Rev.* **1950**, *80(4)*, 580–594.

[25] Carr, H.; Purcell., E. M. *Phys. Rev.* **1954**, *94(3)*, 630–638.

[26] Freeman, R.; Hill., H. D. W. *J. Chem. Phys.* **1971**, *54(1)*, 301–313.

[27] Solomon., I. *Phys. Rev.* **1958**, *110(1)*, 61–65.

[28] Meiboom, S.; Gill., D. *Rev. Sci. Instrum.* **1958**, *29(8)*, 688–691.

[29] Bodenhausen, G.; Ruben, D. J. *Chem. Phys. Lett.* **1980**, *69(1)*, 185–189.

[30] Paquin, R.; Pelupessy, P.; Duma, L.; Gervais, C.; Bodenhausen, G. *J. Chem. Phys.* **2010**, *133*.

[31] Facelli, J. C. *Prog. Nuc. Magn. Reson.* **2011**, *58*, 176–201.

[32] Boyd, J.; Redfield, C. *j. Am. Chem. Soc.* **1998**, *120*, 9692–9693.

[33] Cisnetti, F.; Loth, K.; Pelupessy, P.; Bodenhausen., G. *Chem. Phys. Chem.* **2004**, *5*, 807–814.

[34] Redfield, A. G. *IBM J. Res. Dev.* **1957**, *1*, 19–31.

[35] Wolinski, K.; Hinton, J. F.; Pulay, P. *j. Am. Chem. Soc.* **1990**, *112*, 8251.

[36] Walker, O.; Mutzenhardt, P.; Tekely, P.; Canet, D. *j. Am. Chem. Soc.* **2001**, *124*, 865.

[37] Ravindranathan, S.; Kim, C. H.; Bodenhausen, G. *J. bio. NMR* **2005**, *33*, 163.

[38] Kumar, A.; Grace, R. C. R.; Madhu, P. K. *Prog. Biophys. Mol. Biol.* **2000**, *37*, 191.

[39] Ghalebani, L.; Bernatowicz, P.; Nikkhou-Aski, S.; Kowalewski, J. *Concept. Magn. Reson. A.* **2007**, *30*, 110–115.

[40] Mackor, E. L.; MacLean, C. *Prog. NMR Spectrosc.* **1967**, *3*, 129–157.

[41] Bouguet-Bonnet, S.; Leclerc, S.; Mutzenhardt, P. M.; Canet, D. *J. Magn. Reson.* **2005**, *76*, 4751.

[42] Fukaya, H.; Ono., T. *J. Comp. Chem.* **2004**, *25(1)*, 51–60.

[43] L.K. Sanders, E. O. *J. Phys. Chem. B* **2001**, *105*, 8098.

[44] Cai, S.; Yu, X.; Chen, Z.; Wan., H. *Magn. Reson. Chem.* **2003**,

[45] Harding, M.; Lenhart, M.; Auer, A. *J. Gauss, J. Chem. Phys.* **2008**, *128*, 24.

[46] Elavarasi, S. B.; Dorai, K. *Chem. Phys. lett.* **2010**, *489*, 248–253.

[47] Canet, D. *Prog. NMR Spectrosc.* **1989**, *21*, 237–291.

[48] Canet, D. *Concept. Magn. Reson. A.* **1998**, *10*, 291.